Investigation of Copper Nanoparticle and Bimetallic Catalysts for Electroreduction of Carbon Dioxide

Honors Undergraduate Research Thesis

By

Sean Byrne

Principal Investigator: Dr. Anne Co, The Ohio State University, Department of Chemistry and Biochemistry

April 17th 2017

Abstract

Increasing global population and energy needs are draining sources of fossil fuels at an unsustainable rate and have affected global climate in a shocking manner. The development of renewable energy sources is underway, but these suffer from variable returns. The amount of energy derivable from the sun and wind varies greatly month to month, day to day, and even between day and night. This problem necessitates the development of better energy storage mechanisms, so that excess energy can be captured and used at times when energy production is low. Carbon dioxide (CO_2) electroreduction is a promising solution to these problems. If paired with a renewable energy source, CO_2 electroreduction can store energy in hydrocarbon products via the recycling of CO_2, reducing energy reliance on fossil fuels and curbing net CO_2 emissions. In this project, the reaction products of several copper catalysts were studied using chronoamperometry and the catalysts were characterized using scanning electron microscopy. Four different types of catalysts were studied: ball-milled nanoporous copper catalysts, mortar and pestle ground nanoporous copper catalysts, rhodium copper catalysts, and iridium copper catalysts.

1 Introduction

This chapter will cover the potential impact of this research, the fundamentals of carbon dioxide electroreduction, and the theory behind analytical and characterization techniques used, including chronoamperometry, gas chromatography/mass spectrometry, nuclear magnetic resonance spectroscopy, and scanning electron microscopy.

1.1 Project Significance

The world consumes progressively more power each year, and one problem becomes increasingly significant: carbon dioxide footprint. According to NASA, nine of the ten years with highest global temperatures have occurred since 2000 (the remaining year being 1998).[1] Related to this are rising global carbon dioxide emissions and atmospheric carbon dioxide concentrations; in 1960, the average concentration of CO_2 in the atmosphere was 317 parts per million, and in 2014 it was 399;[2] global CO_2 emissions from fossil fuels have increased from under 10,000 to over 32,000 teragrams (an increase of over 220%, or 22 billion-billions of kilograms).[3] Global temperatures continue to rise as we consume more fossil fuels to meet rising energy demands. It is imperative that we curtail our usage of these fuels, and find suitable replacements that provide net zero carbon dioxide emission energy; we need fuel made from CO_2. CO_2 electroreduction is one sustainable way of making net-zero carbon fuels, which, when combusted, do not increase the net concentration of CO_2 in the atmosphere.

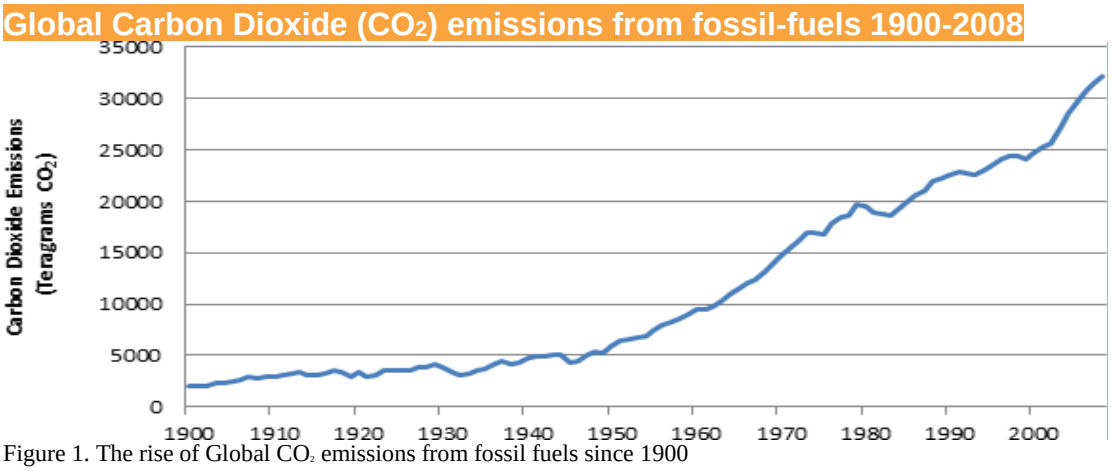

Figure 1. The rise of Global CO_2 emissions from fossil fuels since 1900
Source: Boden, T.A., G. Marland, and R.J. Andres. 2010. Global, Regional, and National Fossil-Fuel CO_2 Emissions. Carbon Dioxide Information Analysis Center, Oak Ridge National Laboratory, U.S. Department of Energy, Oak Ridge, Tenn., U.S.A. doi 10.3334/CDIAC/00001_V2010

1.2 CO_2 Electroreduction

Carbon dioxide electrocatalysis via copper catalysts is one method by which electrical energy can be stored in chemicals. The process involves applying a voltage across an electrical cell, powering aqueous reactions at the catalytic copper surface whereby CO_2 molecules gain energy through reactions, producing molecules of the form $C_xH_yO_z$ that can be combusted as fuel. While other metals may also be used to reduce CO_2, prior studies have shown that copper based materials have high selectivity for useful products.

The electrocatalytic value of copper has long been recognized. One of the first papers on CO_2 electroreduction, published in 1985, discussed the products and associated efficiencies produced by different metal catalysts. In this study, only four products were observed: formate, hydrogen gas, carbon monoxide, and methane. Ten different metal catalysts were used, with vastly different product distributions. Out of the ten, copper was by far the most successful at making methane, the furthest reduced of the products, with a near forty percent efficiency.[4] Five of the others produced mainly formate, two produced carbon monoxide, and the last two produced hydrogen gas.[4] In the thirty intervening years, further research has shown that simple copper foil can produce a variety of products other than methane; a study published in the Royal Society of Chemistry in 2012 observed the presence of sixteen different reduction products reduced by electropolished copper foil.[5] The products observed in the course of these

experiments include hydrogen gas, carbon monoxide, ethane, ethylene, methane, methanol, ethanol, propanol, formate, and acetate.

An ideal catalyst would produce useful products with a high selectivity, work at a low overpotential, have a high current density, a long lifetime, and be cheap to produce. This project is most concerned with selectivity, overpotential, and current density. Among the products listed, alcohols are the most desirable because of their high degree of reduction and energy density. Liquid products are much easier to store than gases, and less combustible. In this project, selectivity is measured using Faradaic Efficiency. Faradaic Efficiency is the percentage of energy that is consumed by the cell that goes into making each product. For example, if the cell consumes 100 Coulombs of charge and produces an amount of product A that requires 50 C, then product A has a 50% FE. Overpotential is the magnitude of voltage applied across the cell, and is an independent variable that is controlled with a potentiostat. Increasing overpotential increases energy input, so a smaller overpotential is generally more energy efficient. Current density relates the rate of the charge being consumed to the surface area of the catalyst. Current is directly related to reaction rate, so a higher current density implies more reactions being completed per unit time. Current is measured by the potentiostat, and the surface area of the catalyst remains fixed within the physical cell. Lifetime is simply how many reactions the catalyst can catalyze before becoming inert, and was not directly measured by this experiment. Costs to produce these catalysts derive from copper prices, the cost of buying or producing copper nanoparticles, and the metal salts which are used to make bimetallic catalysts. Costs have not been calculated, as the main goal of this project was to identify effective catalysts more so than cheap ones.

1.3 Previous Work

The experimental setup used in this project was developed by Joshua Billy, a graduate student in the Co research lab. His experiments included tests of electropolished copper without the deposition of copper nanoparticles, the results of which are listed in figure 2. These experiments

were done with a couple changes in the method, including flowing the electrolyte solution through the working compartment and holding the potential for twice as long. At -1.15 V the electropolished foil produced hydrogen, carbon monoxide, methane, ethylene, formate, and in one case methanol. At -1.35 V, hydrogen, carbon monoxide, methane, ethylene, a very small amount of ethane, formate, ethanol, and propanol were produced.

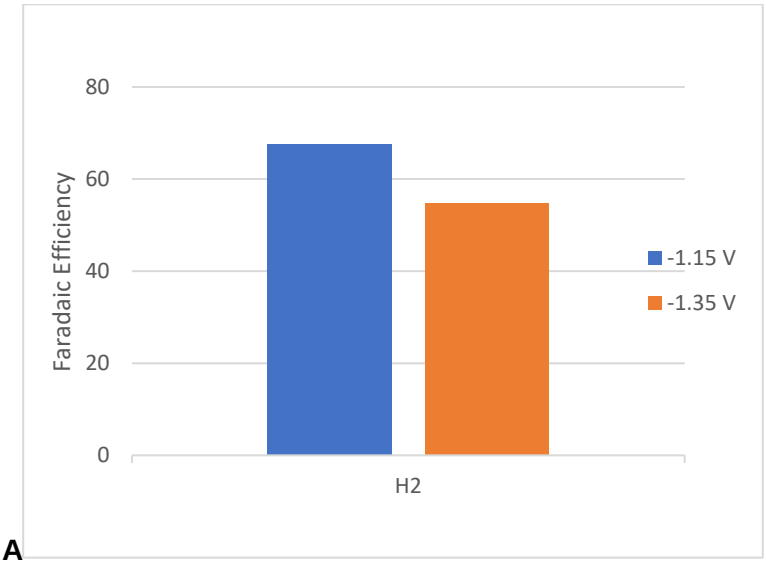

A

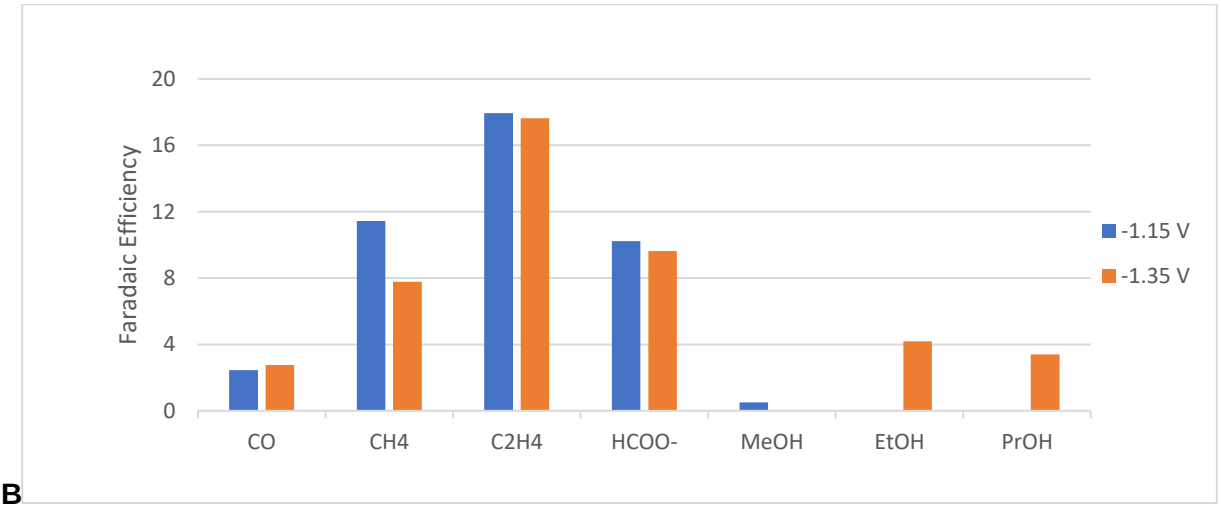

B

Figure 2: graphs of product selectivity in Faradaic Efficiency for polished copper foil collected by Joshua Billy. Experiments were done at room temperature using 0.1 M $KHCO_3$ as an electrolyte, flowing through both the counter and working compartments. The catalytic surface area was 26 cm^2, DSA was used as a counter electrode, and RHE was used as a reference.

1.4 Gas Chromatography/Mass Spectrometry

Gas chromatography/Mass Spectrometry was used in this experiment to measure the gaseous products produced by the reaction. Gas chromatographs separate small gas samples into their constituent analytes using a long tubular column through which gas molecules diffuse. At the end of the column lies a detector, which is used to quantify the amount of analyte coming through. In this experiment, gas chromatography was paired with mass spectrometry to facilitate analyte identification. After analytes diffuse through the gas chromatograph they are injected into the mass spectrometer. Here they are ionized and shot through a mass analyzer, which separates out particles based on their mass/charge ratio. These particles are then detected and recorded. A spectrum is then produced which shows the relative frequencies of particles at different mass/charge ratios, which is used to identify the analyte. Because of the specificity in mass/charge measurement and fragmentation patterns of analytes (due to ionization), mass spectrometry is a very reliable way of identifying analytes.

1.5 Nuclear Magnetic Resonance Spectroscopy

Nuclear magnetic resonance (NMR) spectroscopy allows analytes to be identified by providing information about certain elements present in the sample. Proton NMR was used in this project to detect and quantify liquid reaction products. NMR spectrometers apply strong magnetic fields to a sample, which causes spins of the hydrogen nuclei to align in the same or opposite direction of the field. These two states differ in energy, and manipulating the magnetic field causes some nuclei to change their spin states, releasing energy in the form of photons, which are detected by the NMR spectrometer. Spectra are prepared which measure the frequency and counts of these photons. The peaks produced are characteristic of the compounds which produced them. In addition, the area of the peaks is directly related to the amount of analyte present, so comparing experimental signals to calibrations yields concentration information in the samples.

1.6 Scanning Electron Microscopy

Scanning electron microscopy (SEM) produces high resolution images by exposing a sample to a beam of electrons. The electrons are focused into a small beam that is directed at the sample, where various interactions take place. SEM deals with secondary electrons, which have a low energy, and originate from a thin surface layer of the sample. The energy of these electrons is measured by the instrument, and by probing the surface, an image can be produced.

2 Experimental Section

2.1 Catalyst Preparation

First, discs of copper aluminum alloy (made in house, 17 wt% copper) are heated in 6M NaOH solution at 80 degrees Celsius for 24 hours to remove aluminum. The remaining copper is then soaked in three washes of nanopure water for at least twelve hours each at room temperature. This is then transferred to a tube furnace where it is dried at 400 degrees while flowing hydrogen for 2.5 hours. The heat is turned off and the copper is cooled under hydrogen. For most catalysts, the copper is then ground with mortar and pestle for approximately ten minutes. Three catalysts were prepared with ball-milled copper nanoparticles; catalyst 97A's particles were milled for 5 minutes, 97B's particles were milled for 15 minutes, and 97C's particles were milled for 30 minutes. Solutions of nanoporous copper were prepared by adding approximately 15 mg nanoporous copper to 10 mL methanol. The solutions were degassed in a sonicator for 1 minute and sonicated for 10 minutes. 40 microliters Nafion (Alfa Aesar, PTFE copolymer 5 wt%) were then added, and the solution was sonicated for an additional 10 minutes. This solution was poured on sheets of electropolished copper and evaporated at 80 degrees Celsius. The copper sheets (Aldrich, 0.5 mm thick, 99.98% trace metal) were prepared by electropolishing in concentrated phosphoric acid by application of 1.4 V versus a DSA counter electrode and a platinum wire or Ag/AgCl reference electrode for 10 minutes while stirring. Bimetallic catalysts were prepared by immersing dried nanoporous copper catalysts in $IrCl_3$ or $RhCl_3$ solution for one or three hours while stirring. The catalyst CuIr-Np1 was immersed in 2.5 mM $IrCl_3$ solution for one hour while stirring, while CuIr-Np1 was immersed in 0.25 mM $IrCl_3$ solution while stirring.

2.2 Reaction Cell

The acrylic reaction cell utilizes three electrodes: a copper working electrode (surface area 26 cm^2), a DSA counter electrode, and a reversible hydrogen electrode. The cell contains two electrolyte-filled (0.1 M $KHCO_3$, diluted from electropure 2 M $KHCO_3$) chambers separated by

Selemion, an ion selective membrane. The chamber with the working electrode was continuously saturated with CO_2 using a glass bubbling tube (~9 mL/min). This chamber was connected to the reference electrode through a Luggin capillary and had an outlet to the GC/MS. The second chamber contained the counter electrode, and its electrolyte solution was continuously replenished at 4 mL/min. The reference electrode was platinum mesh in 0.1 M $KHCO_3$ saturated with H_2 gas. A cyclic voltammogram is run from 0 V against the open channel to the experiment's reducing potential at 50 mV/s (a range of -0.85 to -2.05 V). The potential was held for one, two, or three hours in each experiment. All trials were done at room temperature.

2.3 Product Quantification

Gaseous products were carried through the cell to the GC/MS (Agilent 7890A GC, Agilent 5975C MS) by CO_2 bubbled into the working electrode compartment at ~9 mL/min. Gas samples are diverted to the GC/MS every 13 minutes. Liquid samples were collected from the working compartment at the end of the experiment. 800 microliters sample are added to 100 microliters acetonitrile standard (100 ppm) and 100 microliters deuterium oxide. The solution is then run in a 400 MHz NMR using a water-suppressing method. Product peaks are measured and standardized versus the acetonitrile peak, which is held at a constant concentration between experiments. These peaks are converted to ppm measurements using calibration curves created for each product.

3 Results and Discussion: Nanoporous Copper

A number of catalysts prepared with copper nanoparticles were tested. A set of three catalysts using ball-milled copper were compared to investigate a correlation between particle size and product distribution, and these were compared with a thoroughly tested catalyst whose particles were prepared by grinding with mortar and pestle.

3.1 Ball-Milled Nanoporous Copper

Figures 4A-F show the distribution of products for three ball-milled nanoporous copper catalysts. Hydrogen gas was generated in the highest amount. The products carbon monoxide, ethane, ethylene, formate, ethanol, and acetate were produced by each catalyst as well, while propanol was produced only by the 5 minute milled catalyst. Neither methanol nor methane were produced in measurable quantities.

Production of hydrogen gas seems to have no correlation with increased milling, while all other products, including formate, ethane, ethene, ethanol, propanol, and acetate are produced at higher rates by less milled catalysts. There are two other considerations to be made in relation to these trends: first, the sum of the observed products for the 30 minute milled catalyst is lower than the expected sum by 5%, indicating that either product measurements were around 5% below what they should have been, or there are other, unaccounted for products. Secondly, 30 minute milled catalyst produced a current of 0.8393 A, about 5% below the currents of the 5 and 10 minute milled catalysts (0.8821 A and 0.8966 A respectively).

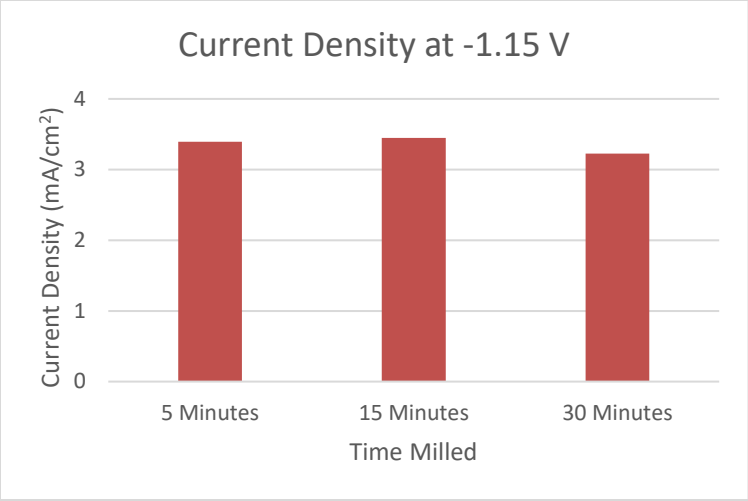

Figure 3: current densities of three ball-milled nanoporous copper catalysts. Experiments were done at -1.15 V at room temperature using 0.1 M $KHCO_3$ saturated with CO_2 gas. The catalyst surface area was 26 cm^2. DSA was used as a counter electrode, and RHE was used as a reference electrode. The current densities are the average from two 60 minute trials of the catalysts.

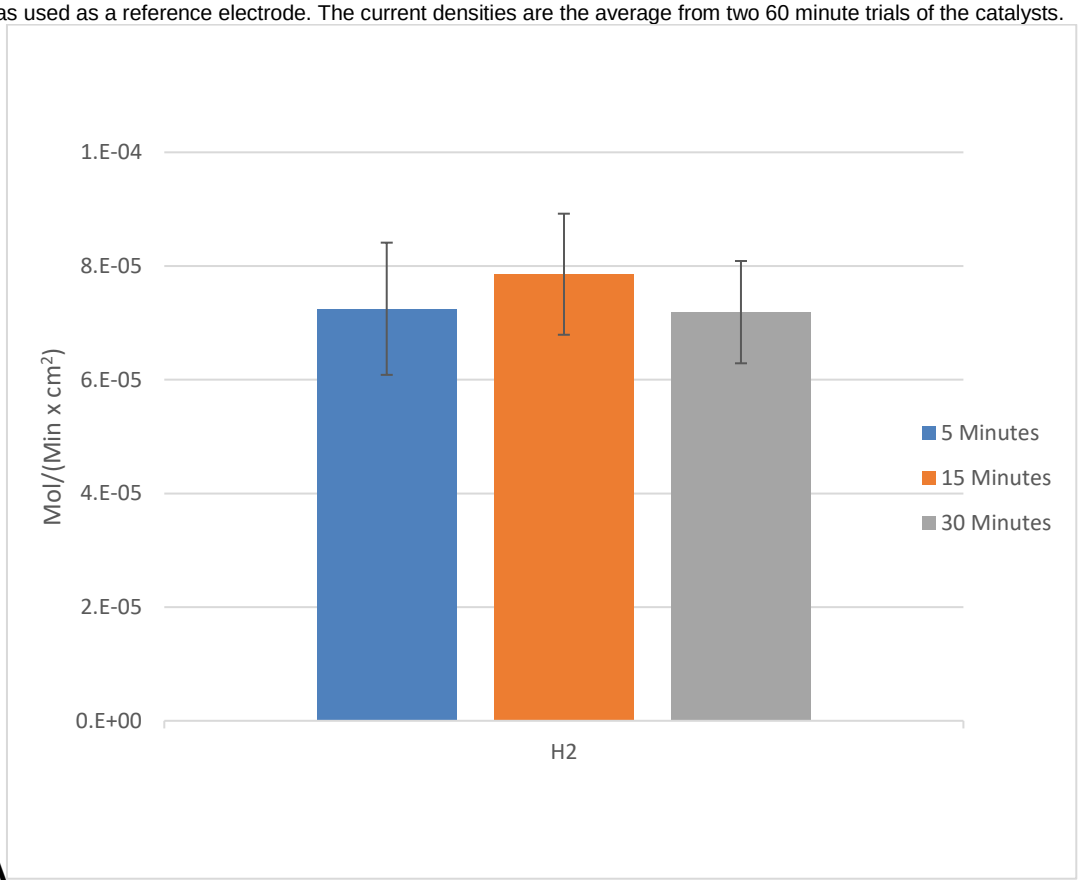

A

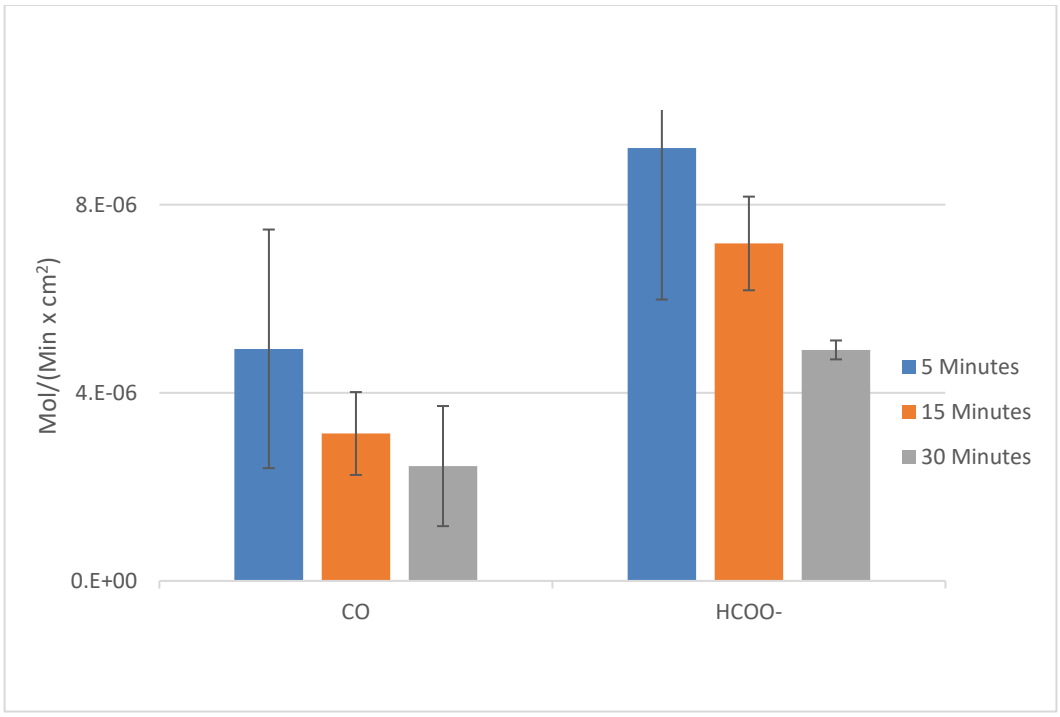
8.E-06
4.E-06
0.E+00
Mol/(Min x cm²)
CO
HCOO-
5 Minutes
15 Minutes
30 Minutes

B

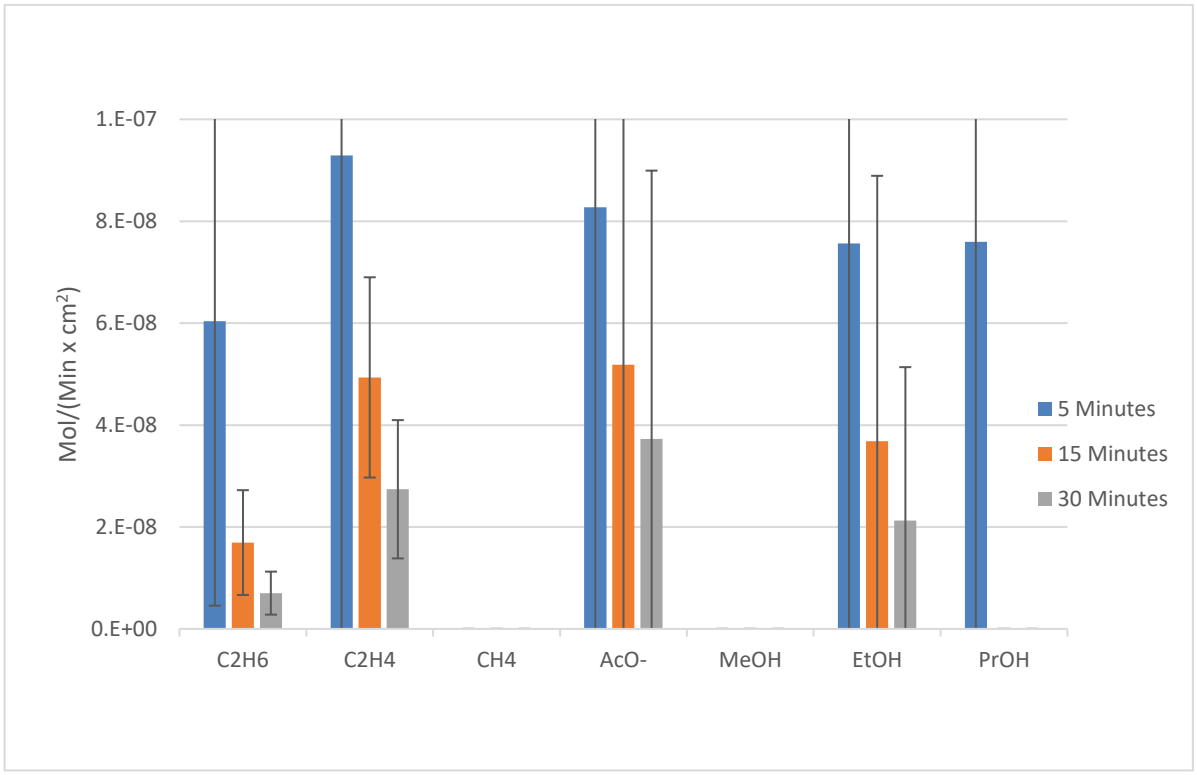
1.E-07
8.E-08
6.E-08
4.E-08
2.E-08
0.E+00
Mol/(Min x cm²)
C2H6
C2H4
CH4
AcO-
MeOH
EtOH
PrOH
5 Minutes
15 Minutes
30 Minutes

C

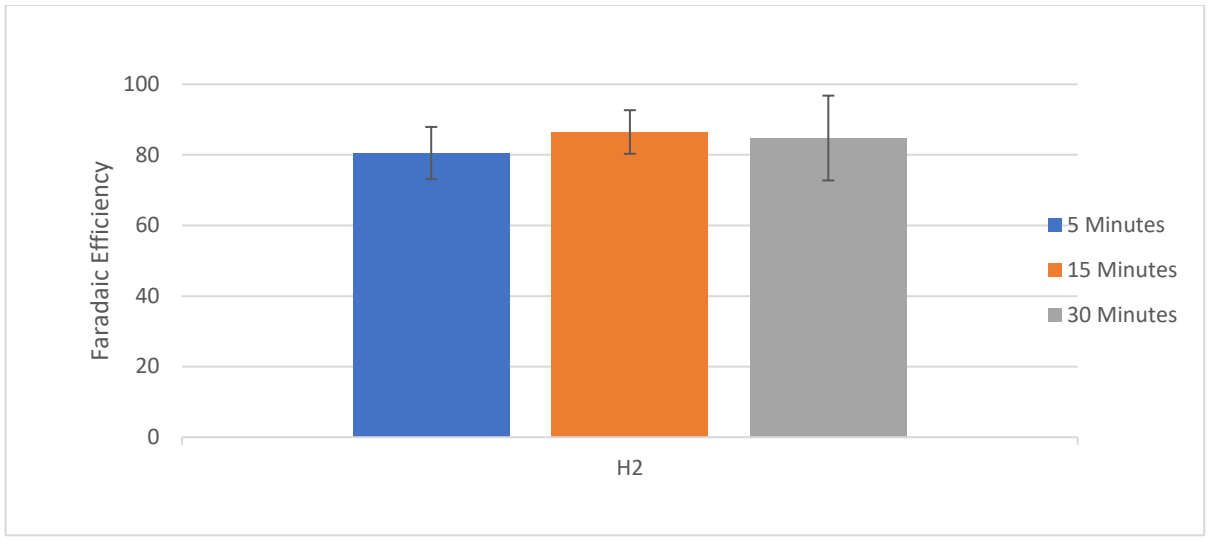
100
80
60
40
20
0
Faradaic Efficiency
H2
5 Minutes
15 Minutes
30 Minutes

D

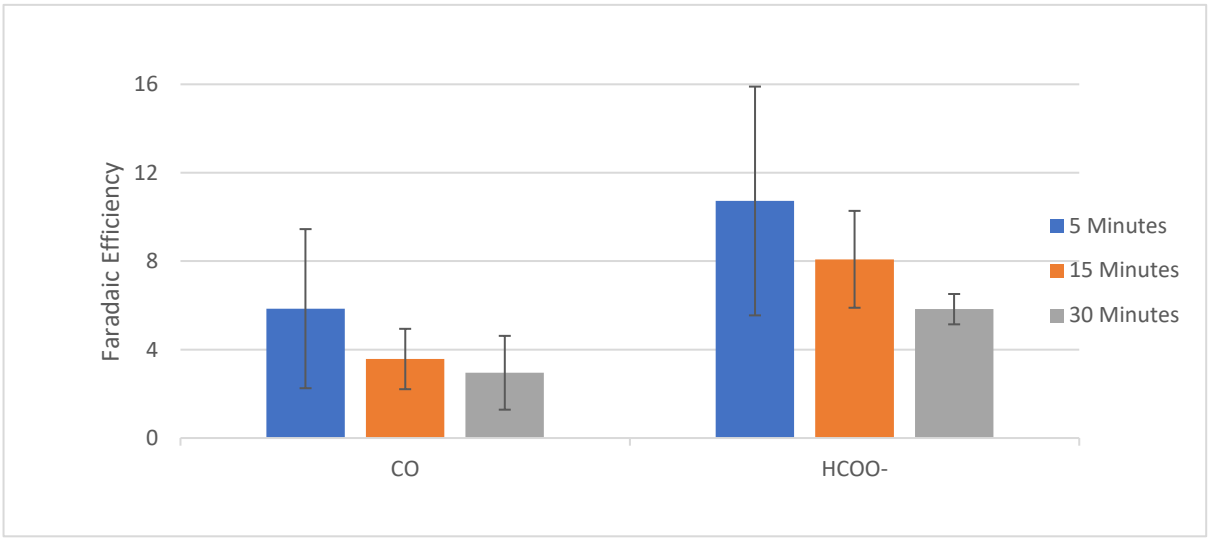
16
12
8
4
0
Faradaic Efficiency
CO
HCOO-
5 Minutes
15 Minutes
30 Minutes

E

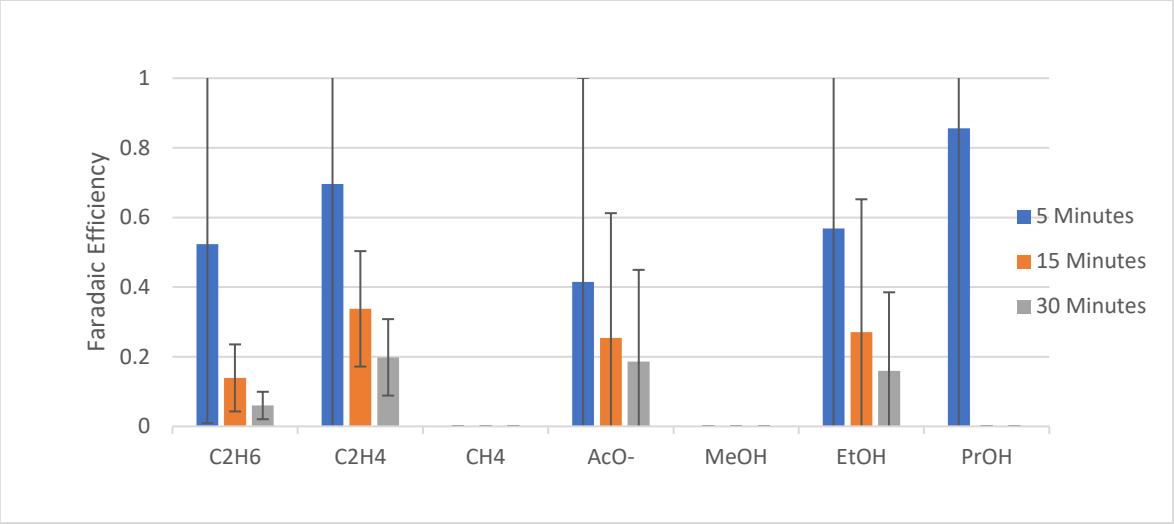

F

Figure 4: the graphs show product distributions of ball-milled catalysts at -1.15 V. Experiments were done at room temperature using 0.1 M $KHCO_3$ saturated with CO_2 gas. The catalyst surface area was 26 cm^2. DSA was used as a counter electrode, and RHE was used as a reference electrode. Graphs A-C measure product formation rates in mol/(min x cm^2), and D-F measure product selectivity using Faradaic Efficiency. Each catalyst was run for two hours cumulatively.

SEM images of these catalysts reveal that more milling correlates with less large structures on the catalyst surface. EDX data from spots on the 5 and 30 minute milled catalysts was also obtained, which showed small amounts of K, C, O, F, and Al. Similar amounts of these elements were found, suggesting that increased milling time did not lead to the incorporation of Si from the glass beads used in milling.

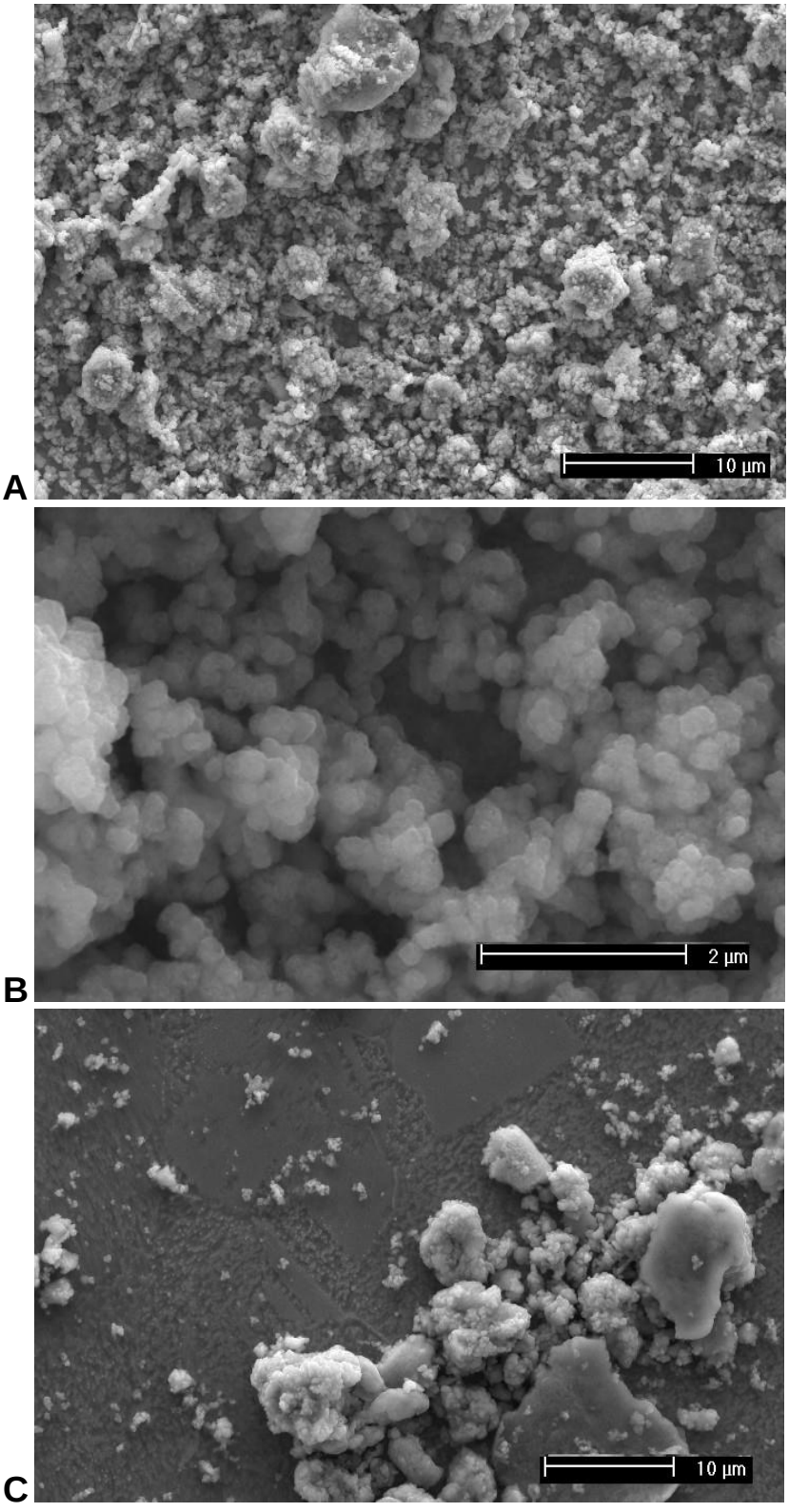
A
10 µm
B
2 µm
C
10 µm

D

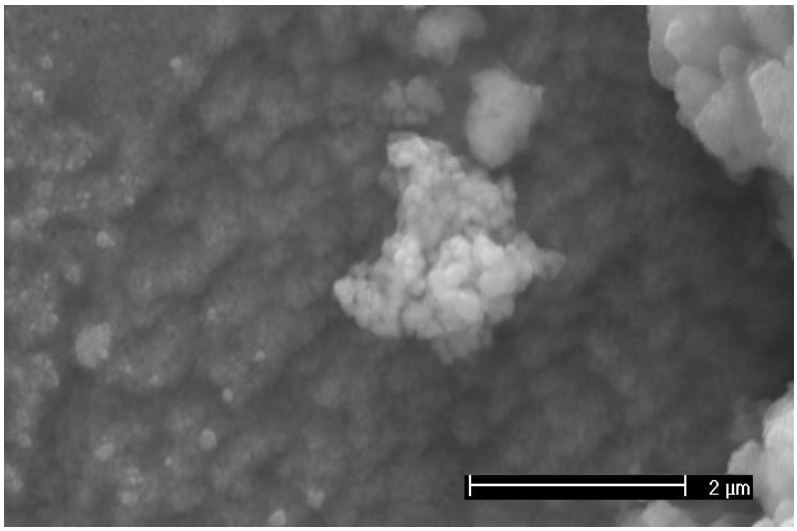

E

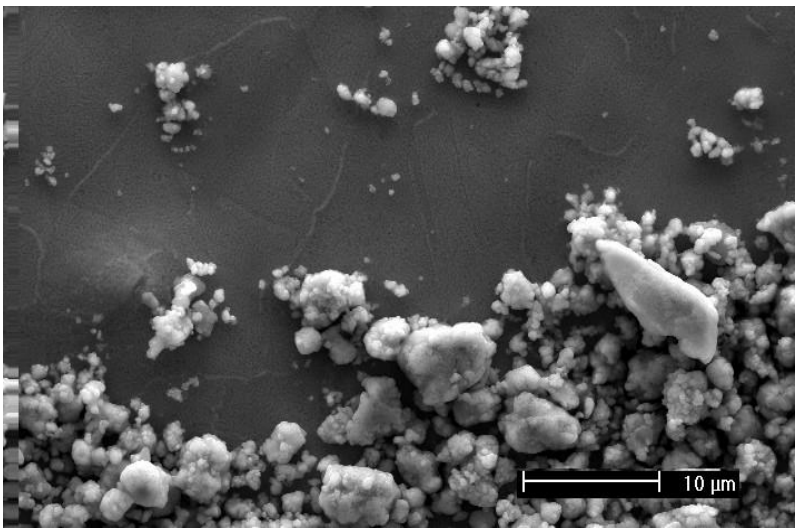

F

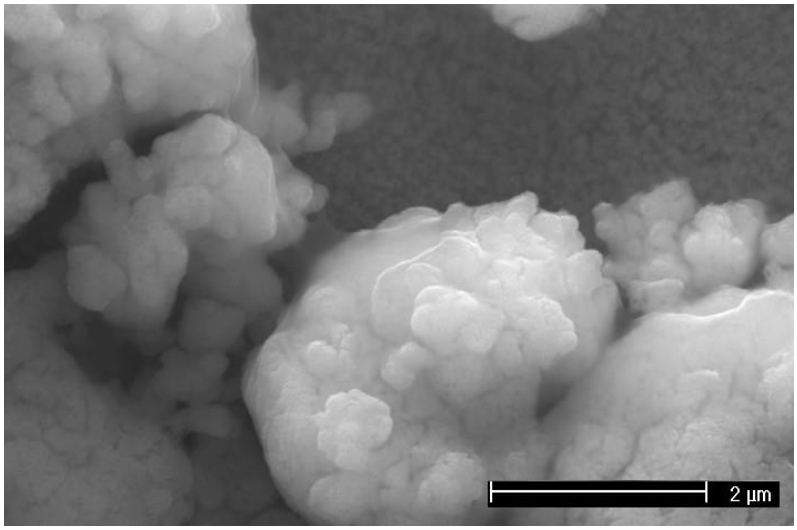

G 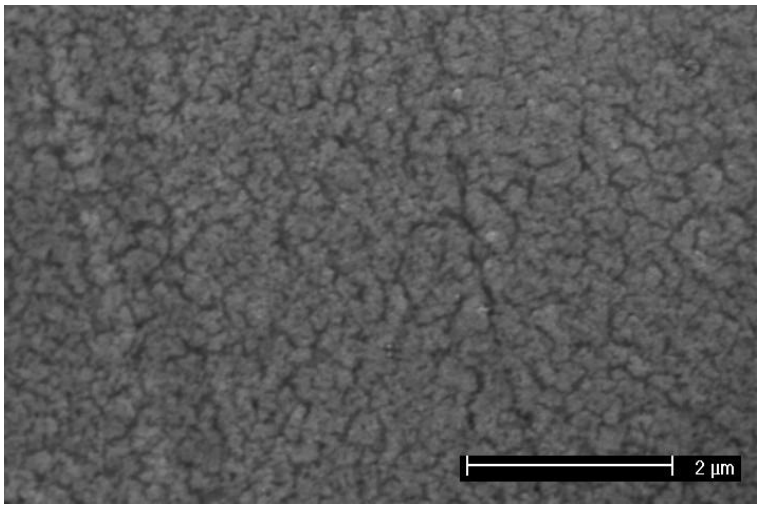

Figure 5: SEM images of ball-milled nanoporous copper catalysts. Each catalyst had been used in 2 hours of experiments. Images A and B are the catalyst milled for five minutes at 1600x and 12800x magnification. Images C and D are the catalyst milled for fifteen minutes at 1600x and 12800x magnification. Images E, F, and G are the catalyst milled for thirty minutes at 1600x, 12800x, and 12800x magnification.

Two general trends existed for the ball-milled nanoporous copper catalysts. The first was that the production of all analytes excluding hydrogen decreased with a higher degree of nanoparticle milling. The second was that hydrogen production correlated with current density. As seen in the above images, the 5 minute milled catalyst's surface was densely covered by clumps of particles that appear uniform in size. The surface floor is almost not visible because of the particles on top of it, and one would expect this coverage to increase surface area to a great extent. However, the current density of this catalyst was less than that of the 15 minute milled catalyst, which looks like it has much less surface area where reactions could take place. Likewise, the current density of the 30 minute milled catalyst is within 10% of the 5 minute catalyst, much higher than would be expected if surface area were directly related to active sites and current. This points to the possibility that the 15 and 30 minute milled catalysts had higher activity for hydrogen, and were able to catalyze more reactions even with less active sites. The electronic properties of metallic nanoparticles are altered because of a lesser degree of superpositioning of wavefunctions. Reduced activity for hydrogen on the 5 minute milled catalyst may be due to the altered electronic properties of the small particles. Hydrogen may be produced at sites on the surface of the catalyst, not at sites on the particulate clumps. Since the 15 and 30 minute milled catalysts allow better access to the surface, this may cause the increased hydrogen production.

The dramatic differences in production for other analytes correlates better with surface area of the catalysts. Although the surfaces of the 15 and 30 minute milled catalysts have similar coverage, their background surfaces differ. Notice that a portion of the 15 minute catalyst's background is rough with mounds. The 30 minute catalyst's background, in contrast, presents a fissured motif across the entire background. It is possible that the mounds on the 15 minute milled catalyst's surface are similar to the particles shown on the 5 minute milled catalyst, and may catalyze reactions of the non-hydrogen products as well.

Interestingly, propanol was only observed as a product in one of the 5 minute milled catalyst's trials, but in none of the 15 or 30 minute milled catalysts' trials. This begs the question, what structures or properties of the 5 minute milled catalyst allowed it to produce propanol, and why only on its second use? The ball-milled copper data, along with that for the catalyst NpCu MP discussed in the next section, suggests that the catalysts consistently produce more products, excluding than hydrogen, on their second use than their first. The possibility of an activation process through catalysis is hinted at by this data, though it was not investigated.

3.2 Mortar and Pestle Nanoporous Copper

As shown in figure 6, the catalyst NpCu MP produced mostly hydrogen at low potentials, with increasing amounts of C_2 and C_3 products at higher potentials. Formate production peaked at -1.55 V, and hydrogen production increased with more negative potential. Carbon monoxide production peaked at -1.35 V, ethane peaked at -1.55 V, ethylene, ethanol, and methane peaked at -1.95 V, methanol reached its highest value at -1.55 V (although it did not have a clear trend between voltages), propanol peaked at -1.75 V, and acetate showed no clear trend, although it was only produced at voltages more negative than -1.35 V.

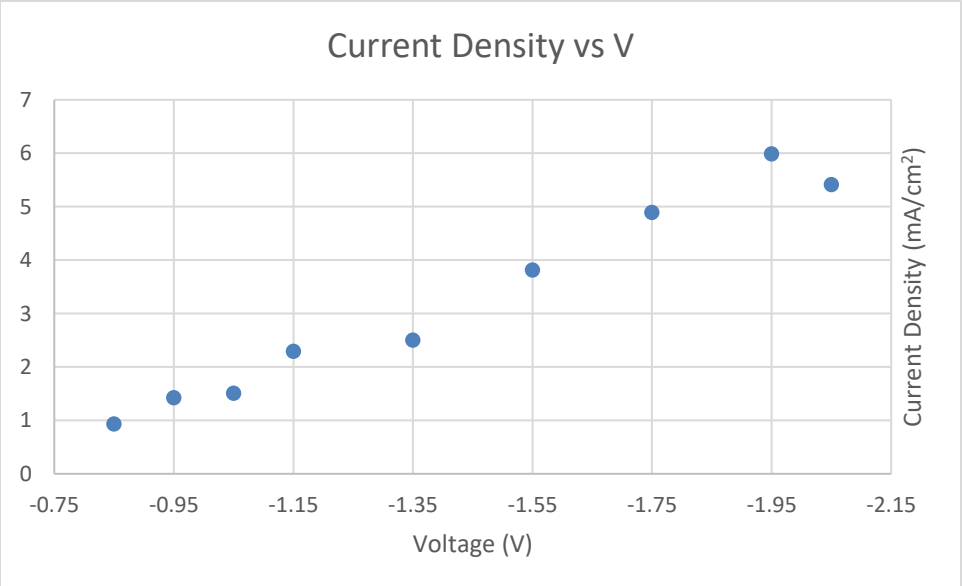

Figure 6: Average current density plotted against voltage for catalyst NpCu MP. Reactions were done at room temperature using 0.1 M $KHCO_3$ saturated with CO_2 gas as electrolyte. Working electrode surface area was 26 cm^2. Experiments were done from -0.85 to -2.05 V. DSA was used as a counter electrode, and RHE was used as a reference.

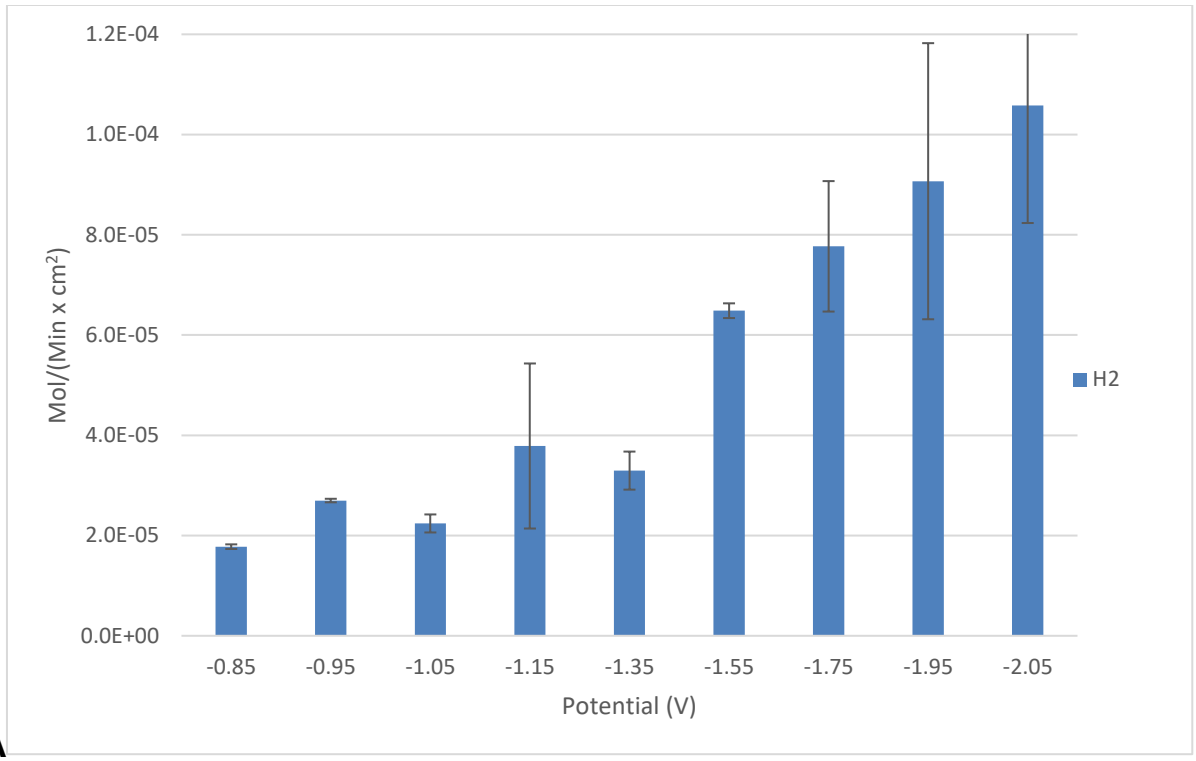
1.2E-04
1.0E-04
8.0E-05
6.0E-05
4.0E-05
2.0E-05
0.0E+00
Mol/(Min x cm²)
H2
-0.85
-0.95
-1.05
-1.15
-1.35
-1.55
-1.75
-1.95
-2.05
Potential (V)

A

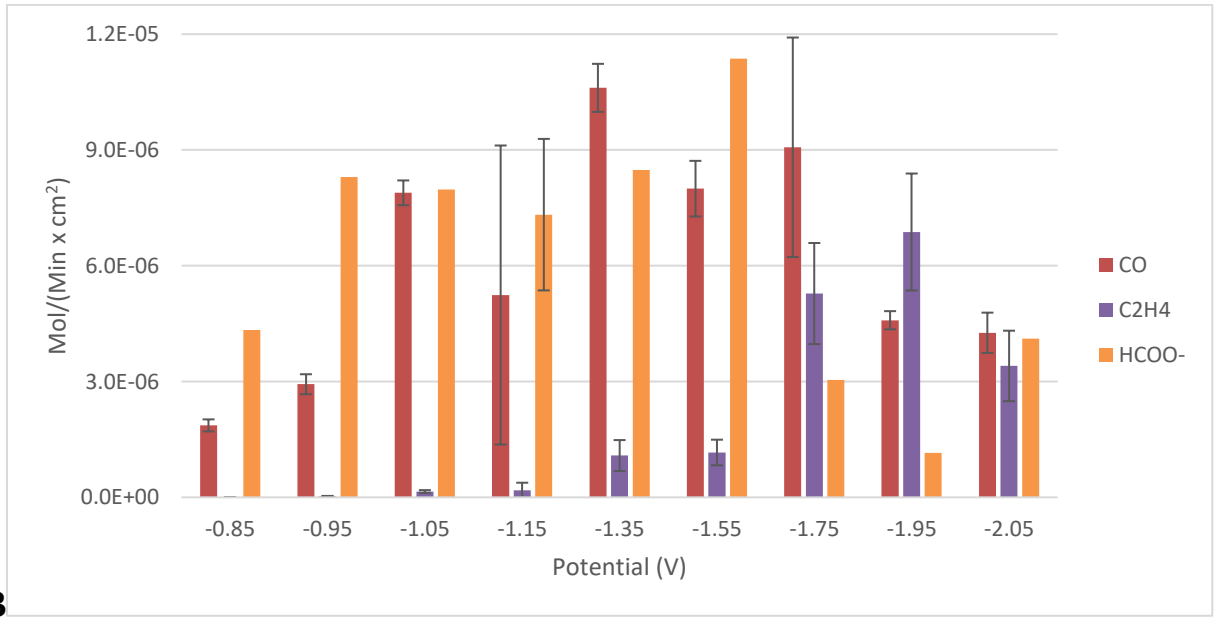
1.2E-05
9.0E-06
6.0E-06
3.0E-06
0.0E+00
Mol/(Min x cm²)
CO
C2H4
HCOO-
-0.85
-0.95
-1.05
-1.15
-1.35
-1.55
-1.75
-1.95
-2.05
Potential (V)

B

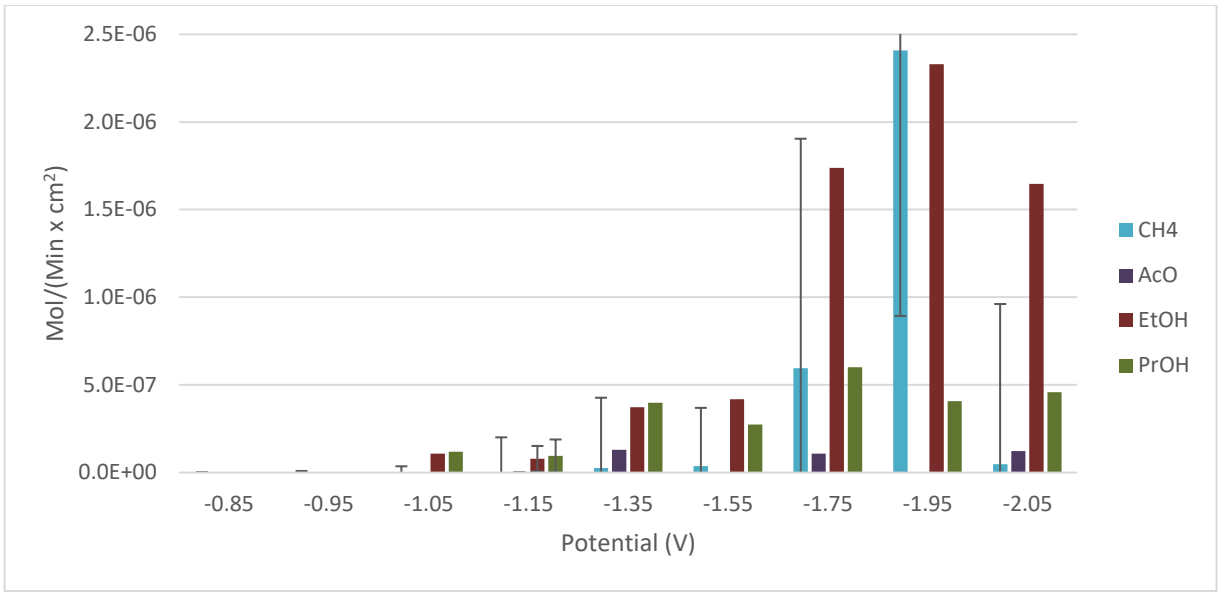
2.5E-06
2.0E-06
1.5E-06
1.0E-06
5.0E-07
0.0E+00
Mol/(Min x cm²)
-0.85
-0.95
-1.05
-1.15
-1.35
-1.55
-1.75
-1.95
-2.05
Potential (V)
CH4
AcO
EtOH
PrOH

C

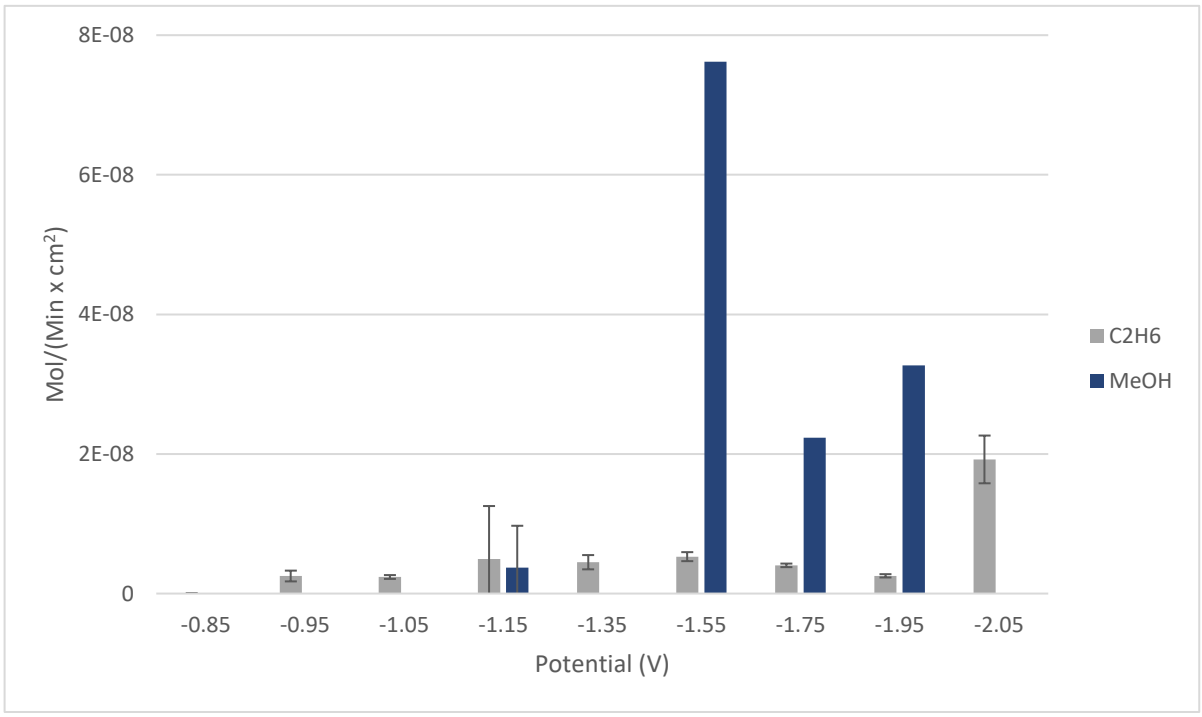
8E-08
6E-08
4E-08
2E-08
0
Mol/(Min x cm²)
-0.85
-0.95
-1.05
-1.15
-1.35
-1.55
-1.75
-1.95
-2.05
Potential (V)
C2H6
MeOH

D

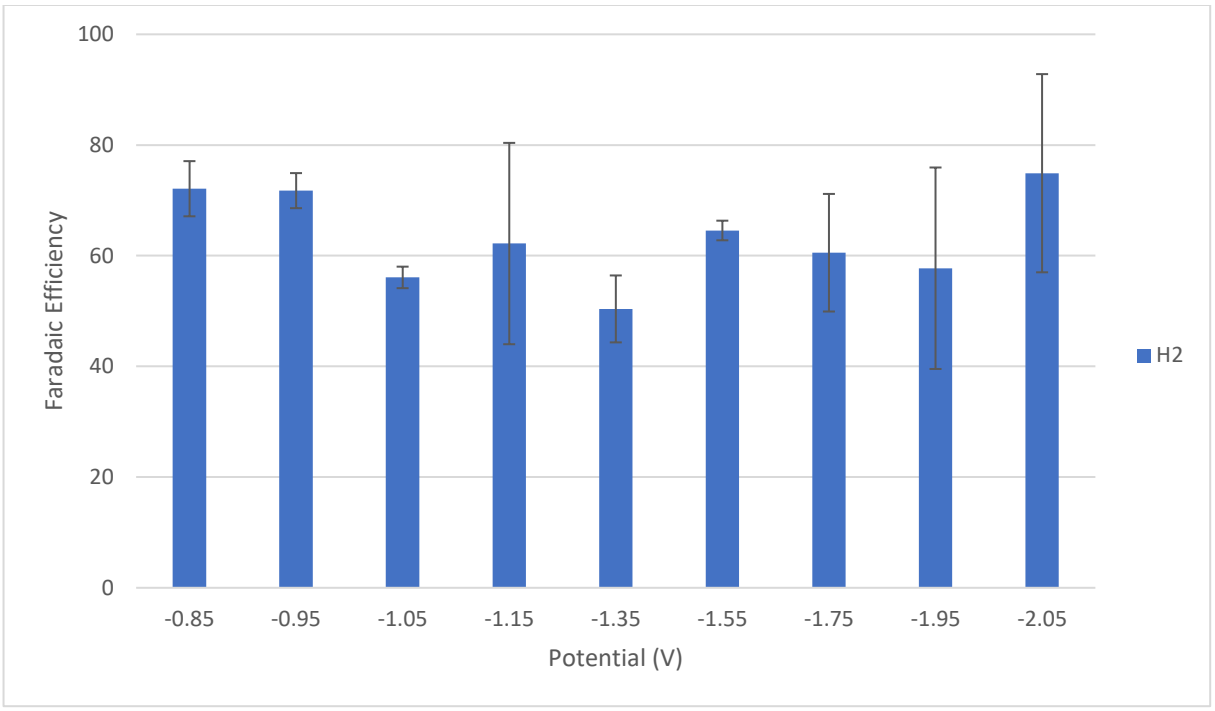
100
80
60
40
20
0
Faradaic Efficiency
-0.85
-0.95
-1.05
-1.15
-1.35
-1.55
-1.75
-1.95
-2.05
Potential (V)
H2

E

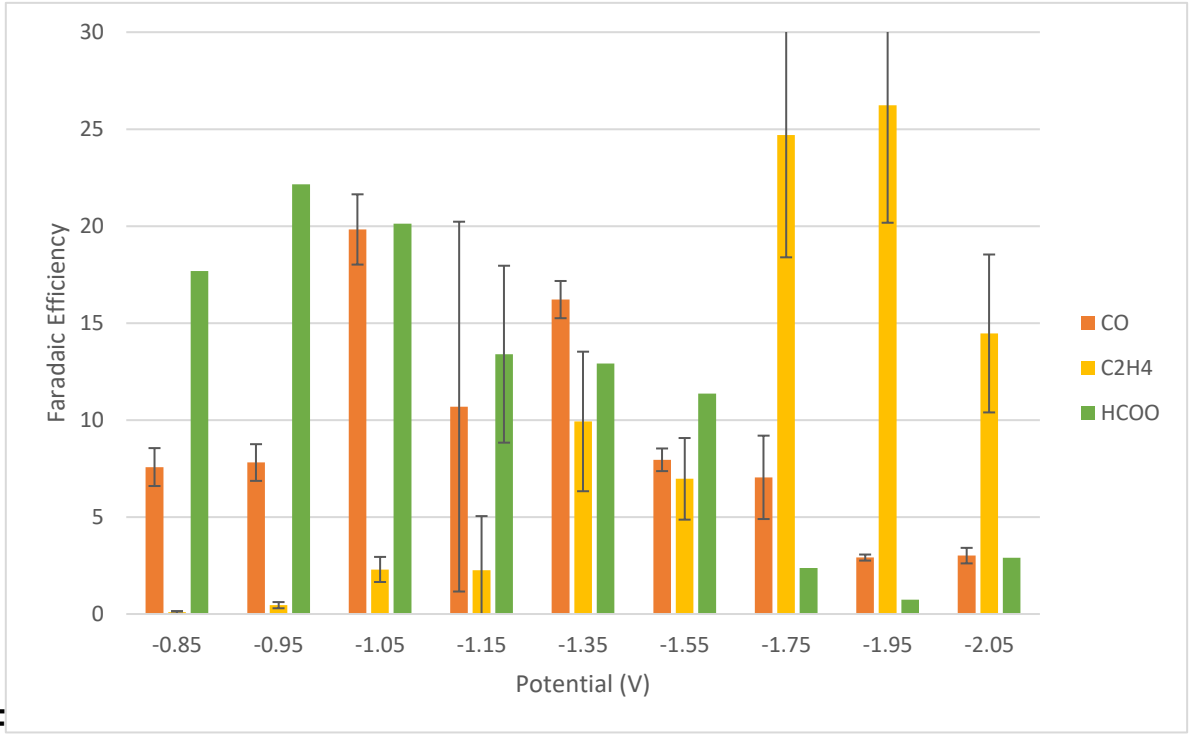
30
25
20
15
10
5
0
Faradaic Efficiency
-0.85
-0.95
-1.05
-1.15
-1.35
-1.55
-1.75
-1.95
-2.05
Potential (V)
CO
C2H4
HCOO

F

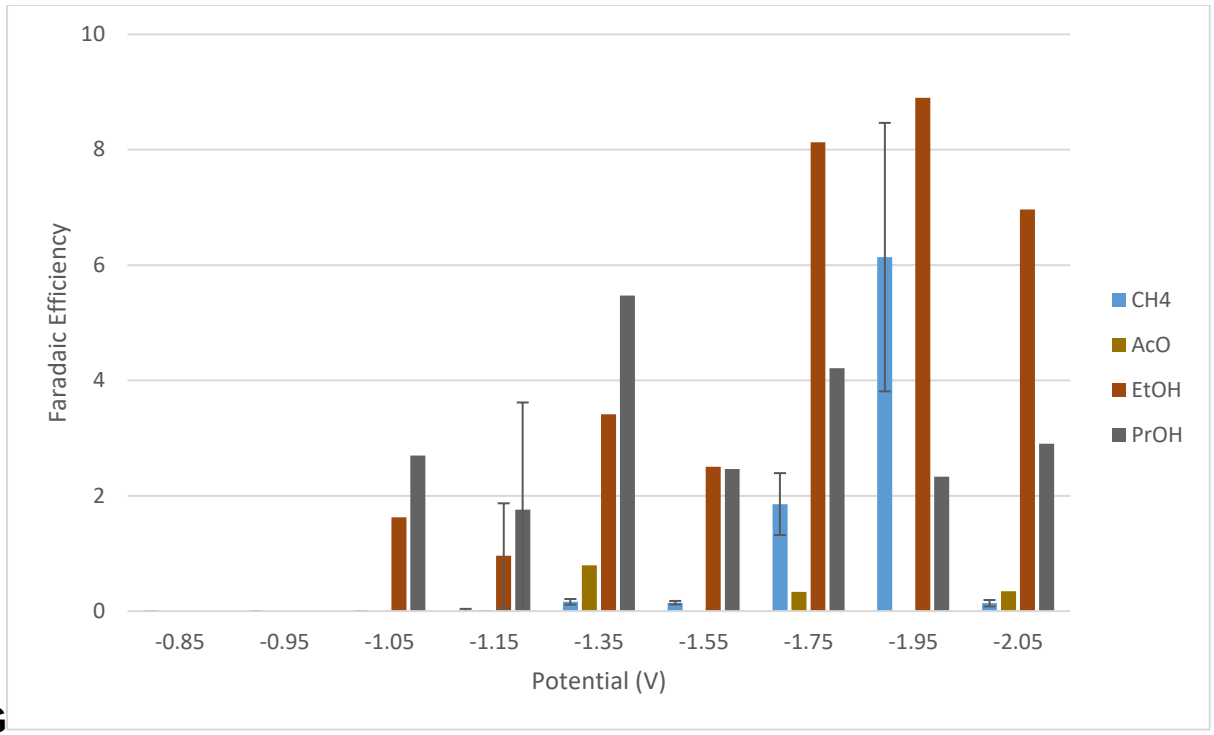

G

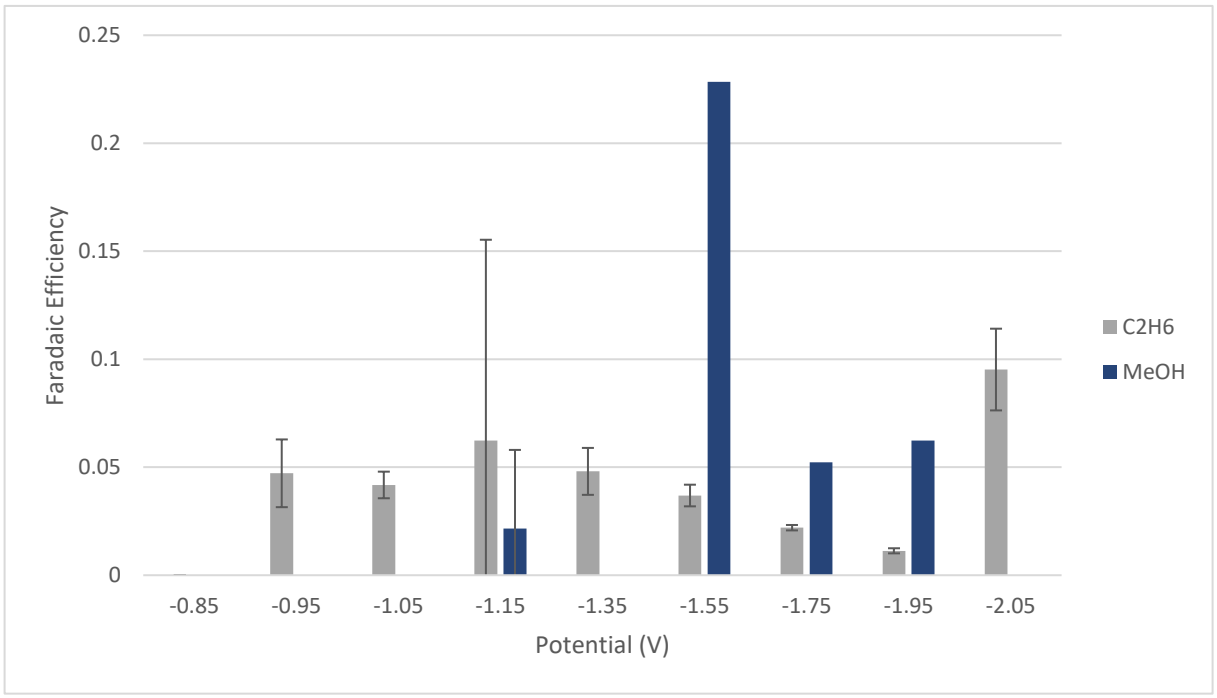

H

Figure 7: graphs A-D present product formation rates in mol/(min x cm^2), and E-H present product selectivity using Faradaic Efficiency for the catalyst NpCu MP. Reactions were done at room temperature using 0.1 M $KHCO_3$ saturated with CO_2 gas. Catalyst surface area was 26 cm^2. Potentials were held for an hour in each experiment. DSA was used as a counter electrode, and RHE as a reference.

Catalyst NpCu MP had very sparse cover of small clumps, and its background was obviously rough. Images at 12800x magnification were also obtained, and revealed finer detail of the clumps and background surfaces. Parts of clumps on the catalyst surface were translucent, as can be seen in image 8A.

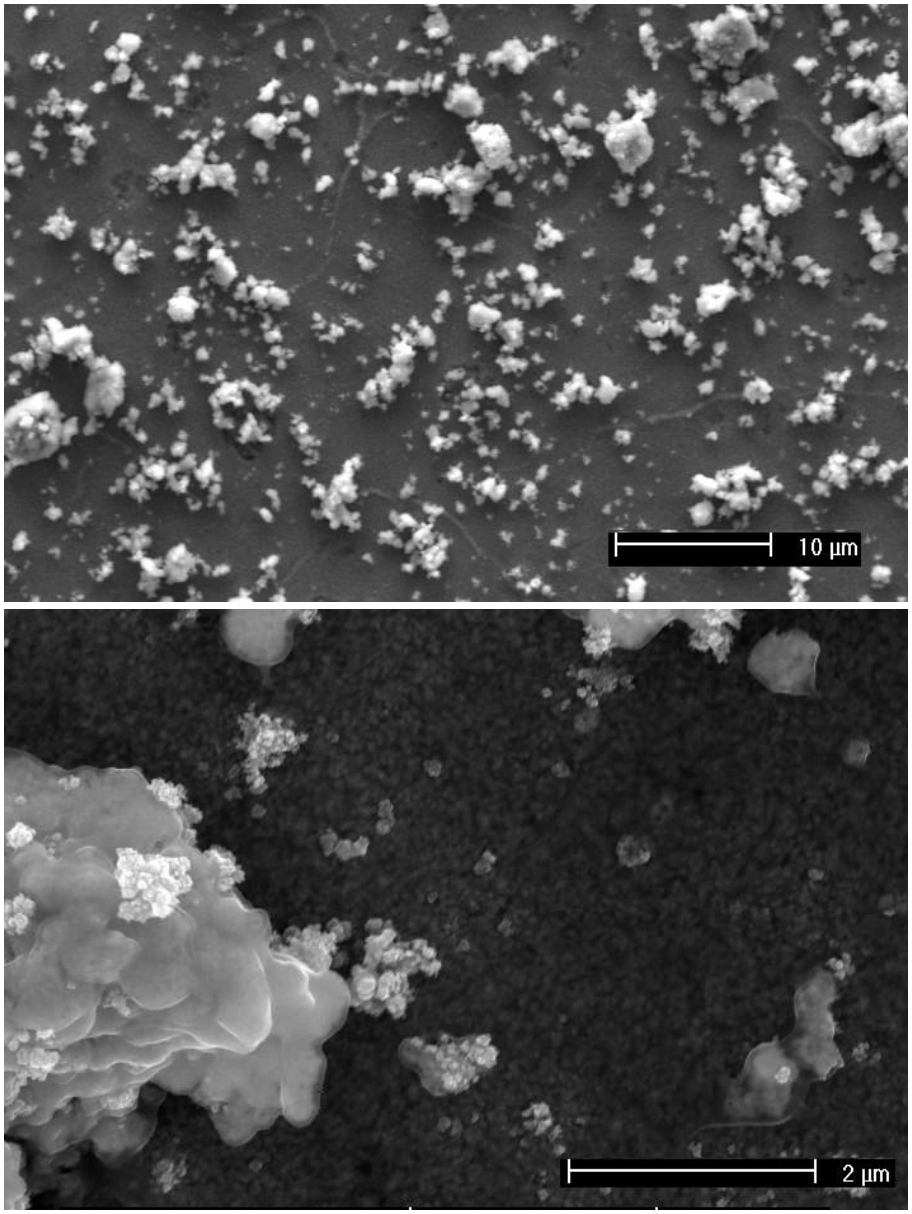

Figure 8: SEM images of catalyst NpCu MP. The catalyst had been used for fifteen hours of experiments. Image A shows 1600x magnification, and image B is 12800x magnification.

The product distribution can be summarized by examining the rates of production based on the number of carbons in the products. For NpCu MP, the C_1 products include carbon monoxide, methane, methanol, and formate. C_2 products include ethane, ethylene, ethanol, and acetate. The only C_3 product detected was propanol. As can be seen in figure 9, C_2 products start to increase as C_1 products decrease. Reaction pathways are an interesting avenue of research in CO_2 electroreduction; it is improbable that propanol, for example, is produced by a single molecule of CO_2 adsorbing to the catalytic surface and undergoing multiple reactions to create propanol at one site. It seems more probable that CO_2 would undergo a simpler reduction and form a more reduced hydrocarbon, which would then adsorb at a different site and undergo further reduction. The data here suggests that at more negative voltages, active sites that catalyze reductions to C_2 products become active, and require C_1 products as reactants, resulting in lower measured levels of C_1 products. This could be further investigated experimentally by running the same experiments but adding ^{13}C labeled reactants to the electrolyte solution. By analyzing ratios of ^{13}C labeled products to normal ^{12}C products, one could draw conclusions about reaction pathways for specific products.

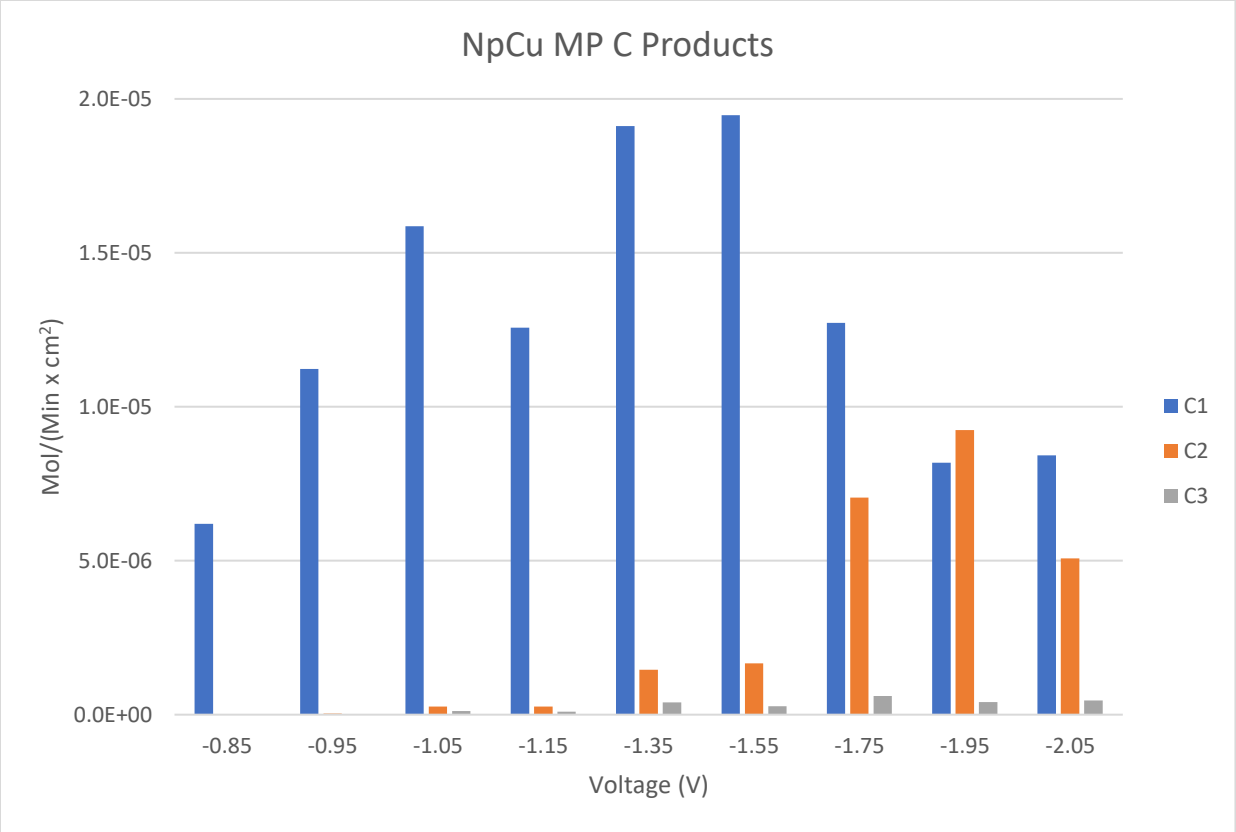

Figure 9: the sums of analyte reaction rates grouped by number of carbon atoms in the product. All reactions were done at room temperature using 0.1 M $KHCO_3$ saturated with CO_2 gas. Catalyst surface area was 26 cm^2, DSA was used as a counter, and RHE was used as a reference.

4 Results and Discussion: Bimetallic Catalysts

Two types of bimetallic catalysts were prepared from simple nanoporous copper catalysts. These were made by immersion of nanoporous copper catalysts in Ir and Rh salt solutions. They were then compared to traditional nanoporous copper catalysts.

4.1 Rhodium Copper Catalysts

Four different rhodium copper catalysts were created. All were made using the same salt solution to displace copper with rhodium, although catalyst CuRh-NpI was immersed in solution for one third the time of the other three catalysts.

Catalyst CuRh-NpI produced hydrogen, methane, ethane, ethylene, carbon monoxide, formate, methanol, ethanol, and acetate. A stopped valve kept gases from being measured in the experiment at -0.85 V, so only liquids were measured. Out of all the products, only hydrogen and formate were produced at over 5% Faradaic Efficiency (FE) in either trial. While current density was higher in the trial at -1.35 V than -0.85 V, both formate and ethanol production stayed the same, while acetate production dropped to zero at -1.35 V, and ethanol was produced only at -1.35 V.

Catalyst CuRh-NpII produced all the same products as NpI with the addition of propanol. In the three trials, only hydrogen, carbon monoxide, and formate were produced at a FE greater than 5%. Due to issues with measuring CO_2 flow rate through the cell for this catalyst's experiments, gas measurements were normalized so that total FE was 100% for each trial, making gas data unreliable. The cell also leaked between the two compartments during the trial at -0.95 V, likely leading to the low current density of that trial. Between the trials at -0.85 and -1.45 V, hydrogen production increased by a factor of three, ethylene increased by a factor of 50, ethane increased by a factor of five, carbon monoxide increased by a factor of five, and formate production stayed constant. Acetate was only produced at -0.95 and -1.45 V, and the alcohols methanol, ethanol, and propanol were only produced at -1.45 V. Methane was only produced in the trial at -0.95 V.

Catalyst CuRh-NpIII produced hydrogen, methane, ethane, ethylene, carbon monoxide, formate, and acetate. Only hydrogen and formate were produced at greater than 5% FE. Hydrogen production dropped slightly between the trials at -0.85 and -0.95 V, but doubled at -1.45 V. Methane was only produced at a small amount at -0.85 V. Ethylene production dropped by a factor of ten between -0.85 and -0.95 V, but doubled between -0.85 and -1.45 V. Ethane was produced at the same rate at -0.85 and -0.95 V, but this rate increased by a factor of seven in the trial at -1.45 V. Carbon monoxide was produced at about the same rate regardless of voltage. Formate production was cut in half between -0.85 and -0.95 V, and was slightly higher at -1.45 V than at -0.85 V. Acetate was only produced at -0.95 V, and methanol was only produced at -0.85 V.

Catalyst CuRh-NpIIIA produced only hydrogen, ethane, ethylene, carbon monoxide, and formate. Hydrogen was produced at just over twice the rate at -0.95 V than at -0.85 or -1.45 V. Ethylene production increased by a factor of 30, but then was cut to half that rate at -1.45 V. Ethane production increased first by a factor of six, then by two. Carbon monoxide nearly tripled between -0.85 and -0.95V, but then dropped slightly at -1.45 V. Formate production tripled from -0.85 to -0.95 V, then increased by 50% at -1.45 V.

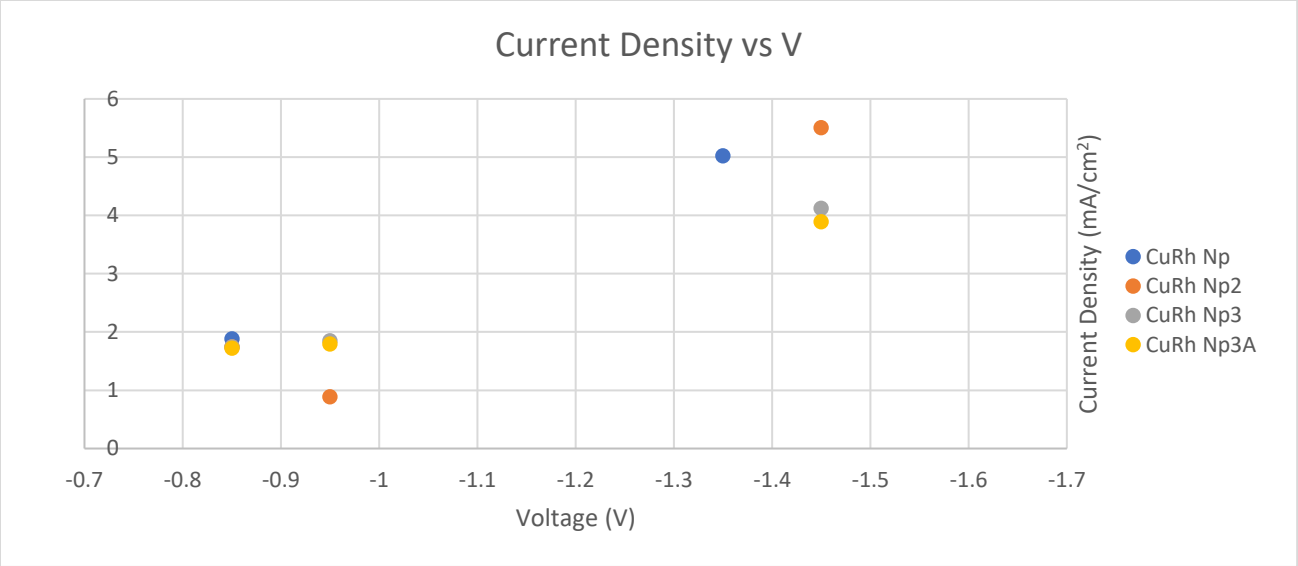

Figure 10: Average current density plotted against voltage for four rhodium copper catalysts. Catalyst surface area was 26 cm^2.

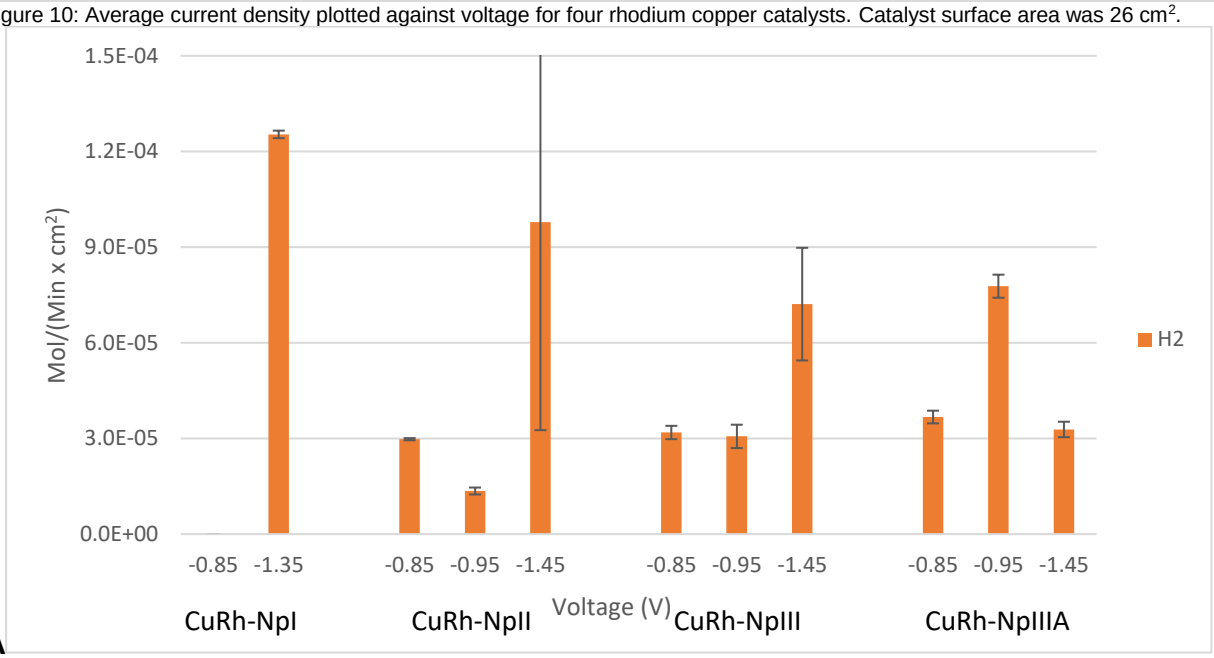

A

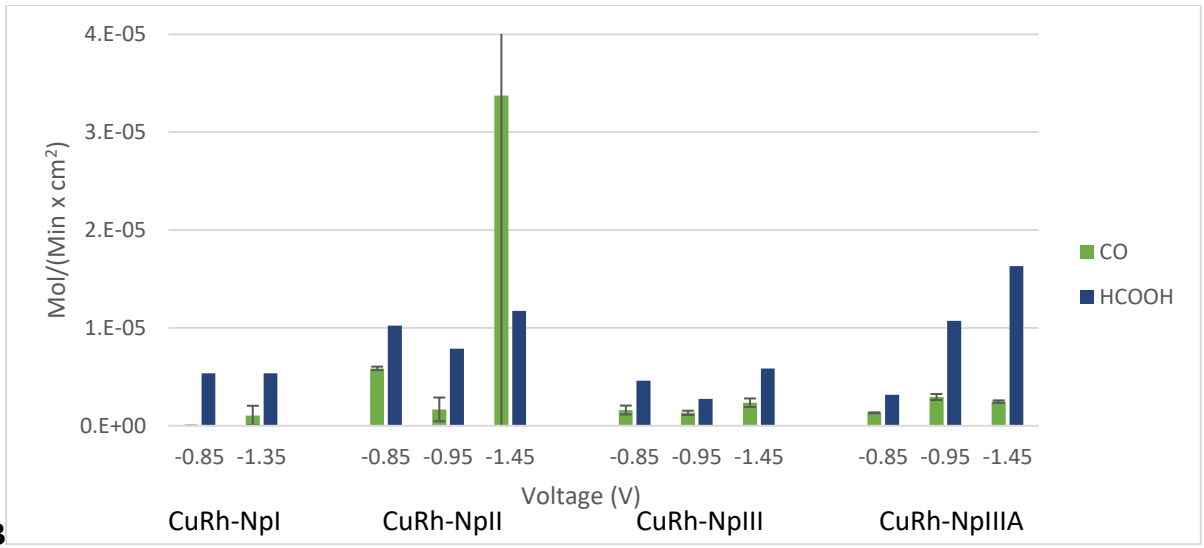
4.E-05
3.E-05
2.E-05
1.E-05
0.E+00
Mol/(Min x cm²)
CO
HCOOH
-0.85 -1.35
-0.85 -0.95 -1.45
-0.85 -0.95 -1.45
-0.85 -0.95 -1.45
Voltage (V)
CuRh-NpI
CuRh-NpII
CuRh-NpIII
CuRh-NpIIIA

B

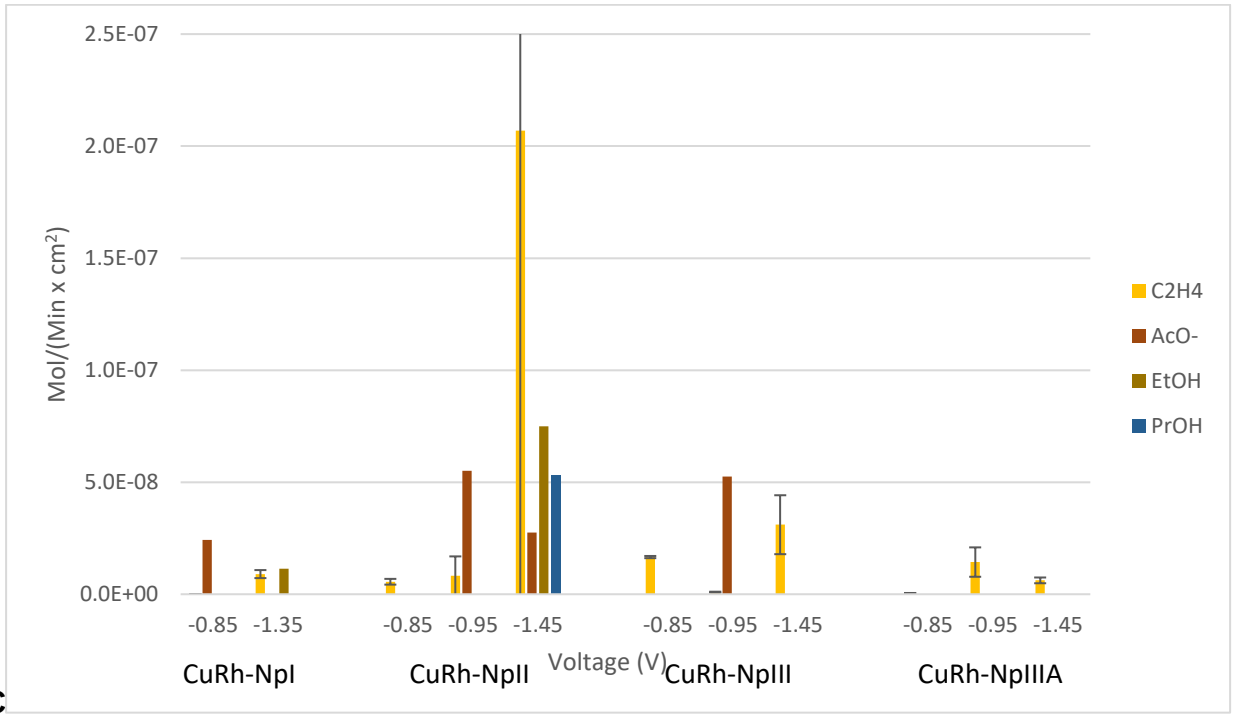
2.5E-07
2.0E-07
1.5E-07
1.0E-07
5.0E-08
0.0E+00
Mol/(Min x cm²)
C2H4
AcO-
EtOH
PrOH
-0.85 -1.35
-0.85 -0.95 -1.45
-0.85 -0.95 -1.45
-0.85 -0.95 -1.45
Voltage (V)
CuRh-NpI
CuRh-NpII
CuRh-NpIII
CuRh-NpIIIA

C

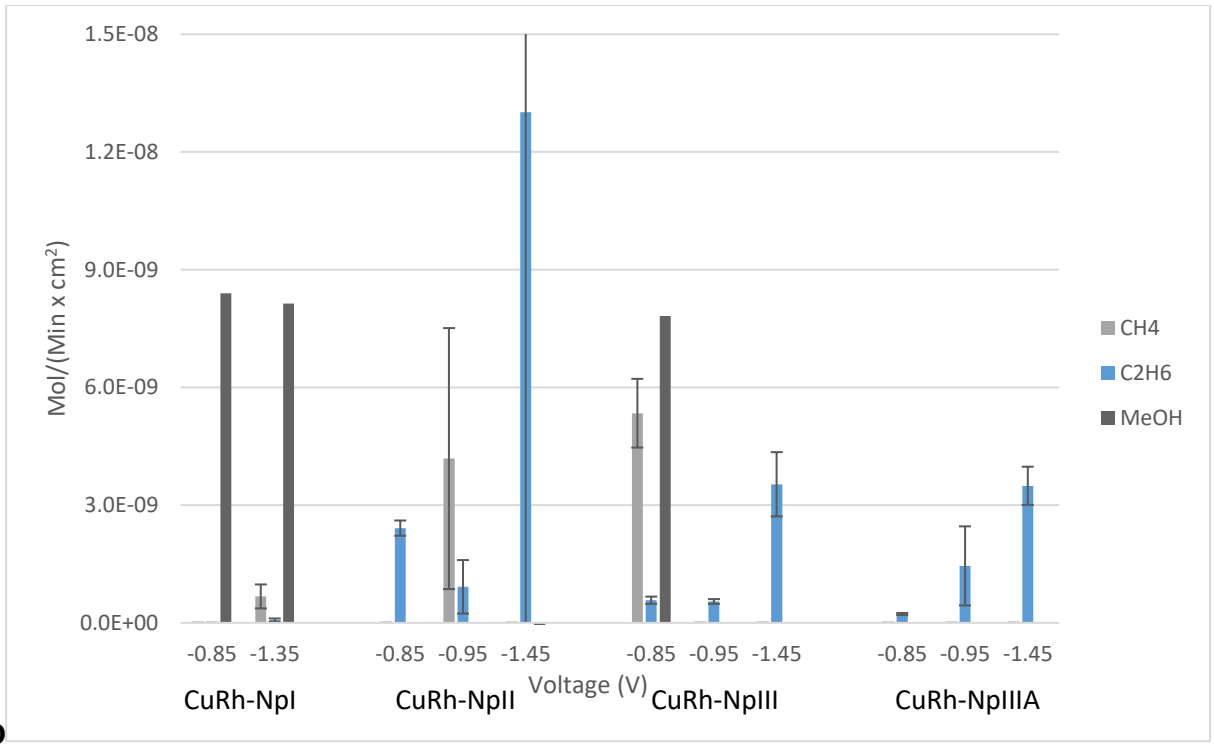
1.5E-08
1.2E-08
9.0E-09
6.0E-09
3.0E-09
0.0E+00
Mol/(Min x cm²)
CH4
C2H6
MeOH
-0.85 -1.35
-0.85 -0.95 -1.45
-0.85 -0.95 -1.45
-0.85 -0.95 -1.45
CuRh-NpI
CuRh-NpII
CuRh-NpIII
CuRh-NpIIIA
Voltage (V)

D

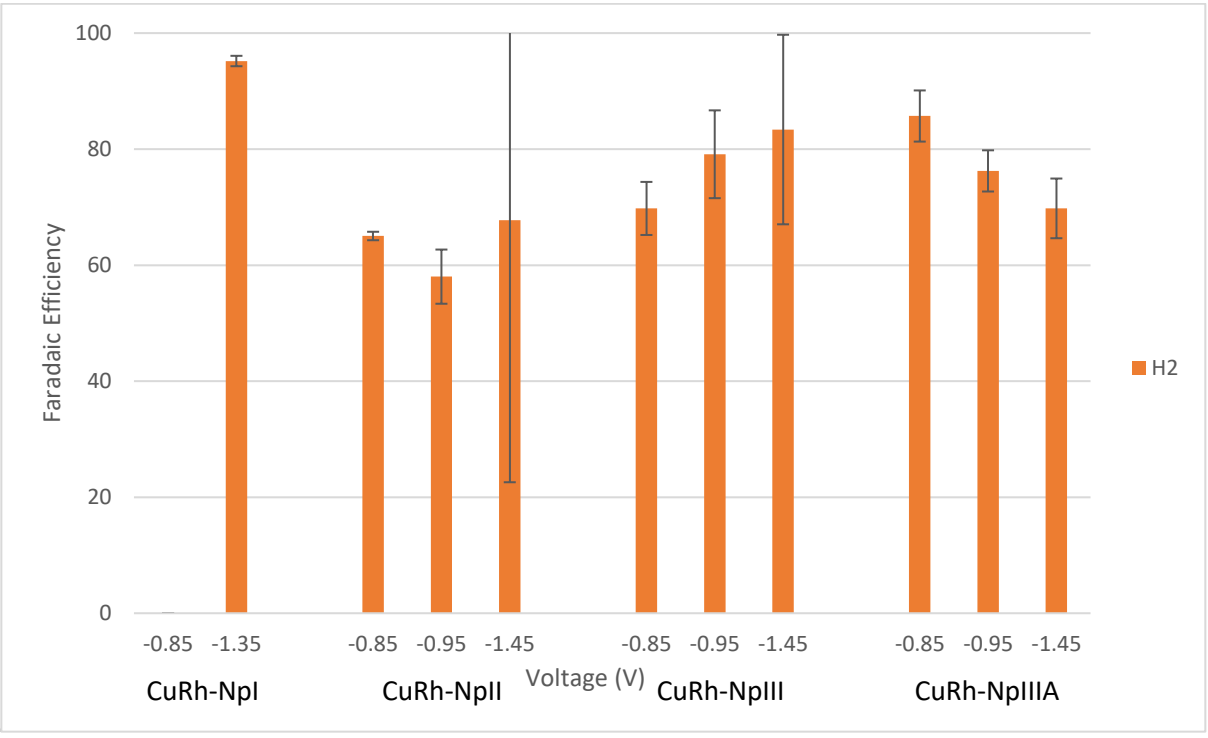
100
80
60
40
20
0
Faradaic Efficiency
H2
-0.85 -1.35
-0.85 -0.95 -1.45
-0.85 -0.95 -1.45
-0.85 -0.95 -1.45
CuRh-NpI
CuRh-NpII
CuRh-NpIII
CuRh-NpIIIA
Voltage (V)

E

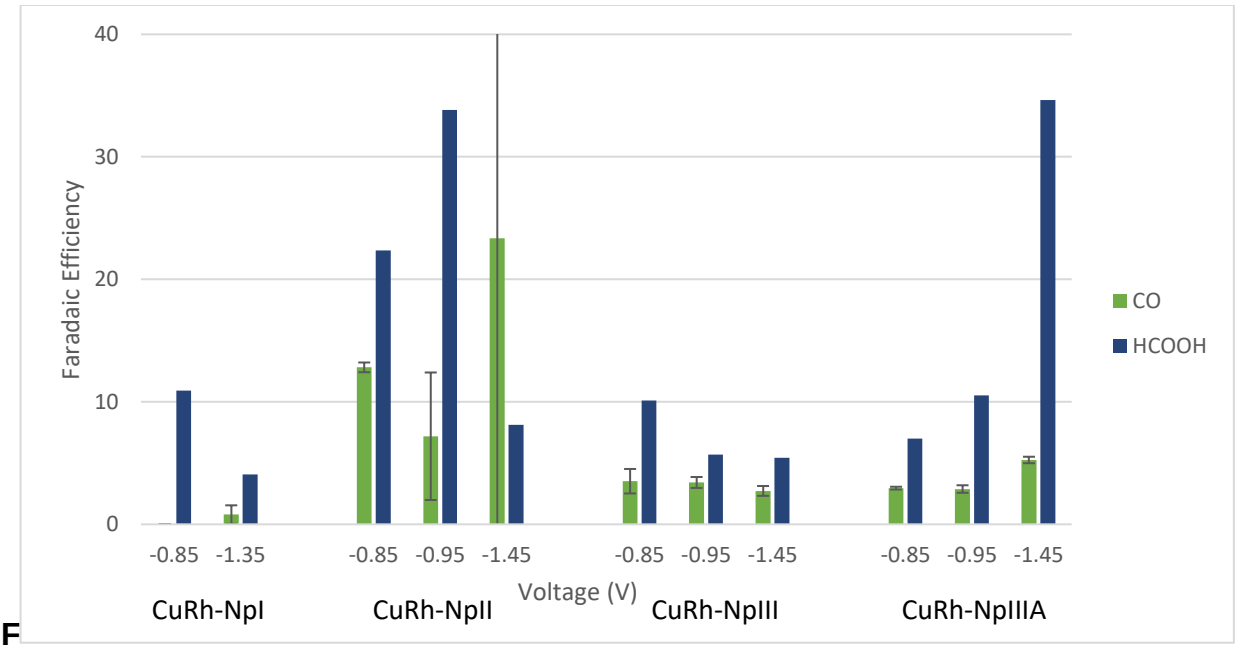
40
30
20
10
0
Faradaic Efficiency
CO
HCOOH
-0.85 -1.35 -0.85 -0.95 -1.45 -0.85 -0.95 -1.45 -0.85 -0.95 -1.45
Voltage (V)
CuRh-NpI
CuRh-NpII
CuRh-NpIII
CuRh-NpIIIA

F

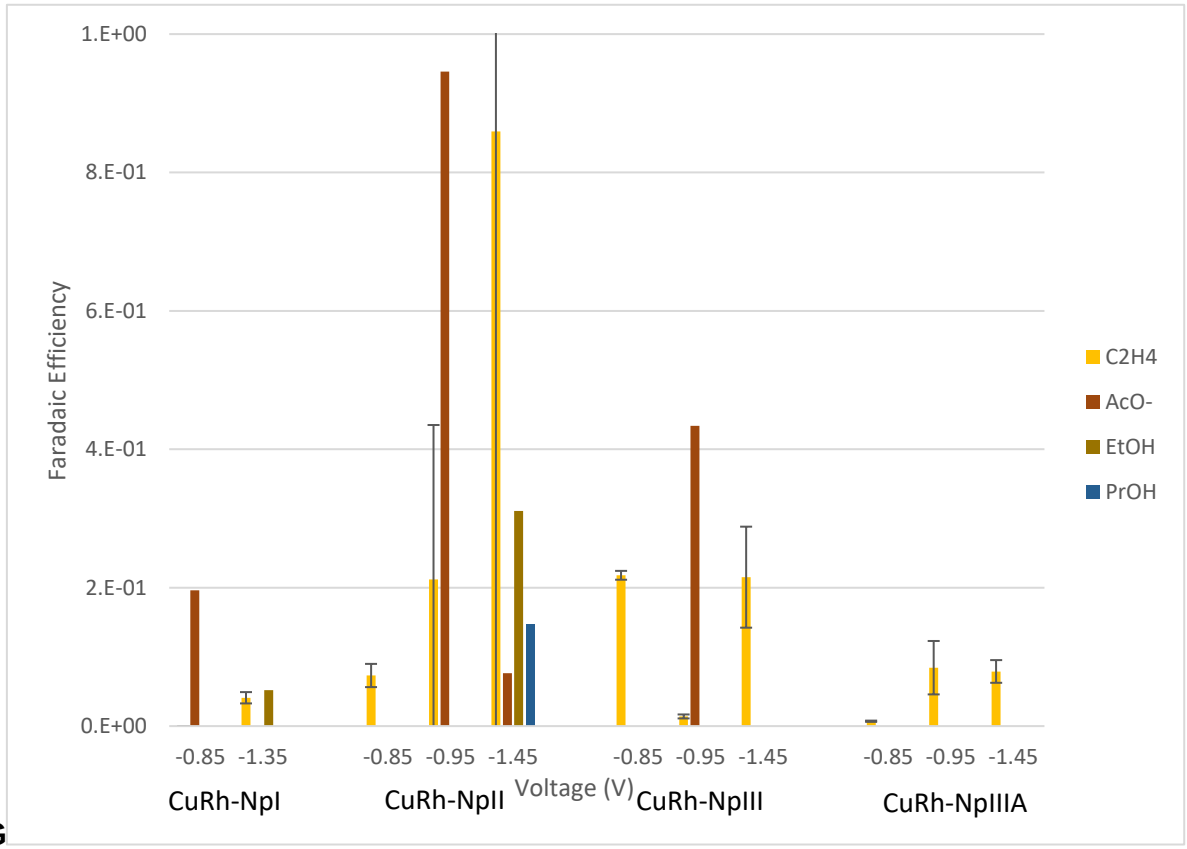
1.E+00
8.E-01
6.E-01
4.E-01
2.E-01
0.E+00
Faradaic Efficiency
C2H4
AcO-
EtOH
PrOH
-0.85 -1.35 -0.85 -0.95 -1.45 -0.85 -0.95 -1.45 -0.85 -0.95 -1.45
Voltage (V)
CuRh-NpI
CuRh-NpII
CuRh-NpIII
CuRh-NpIIIA

G

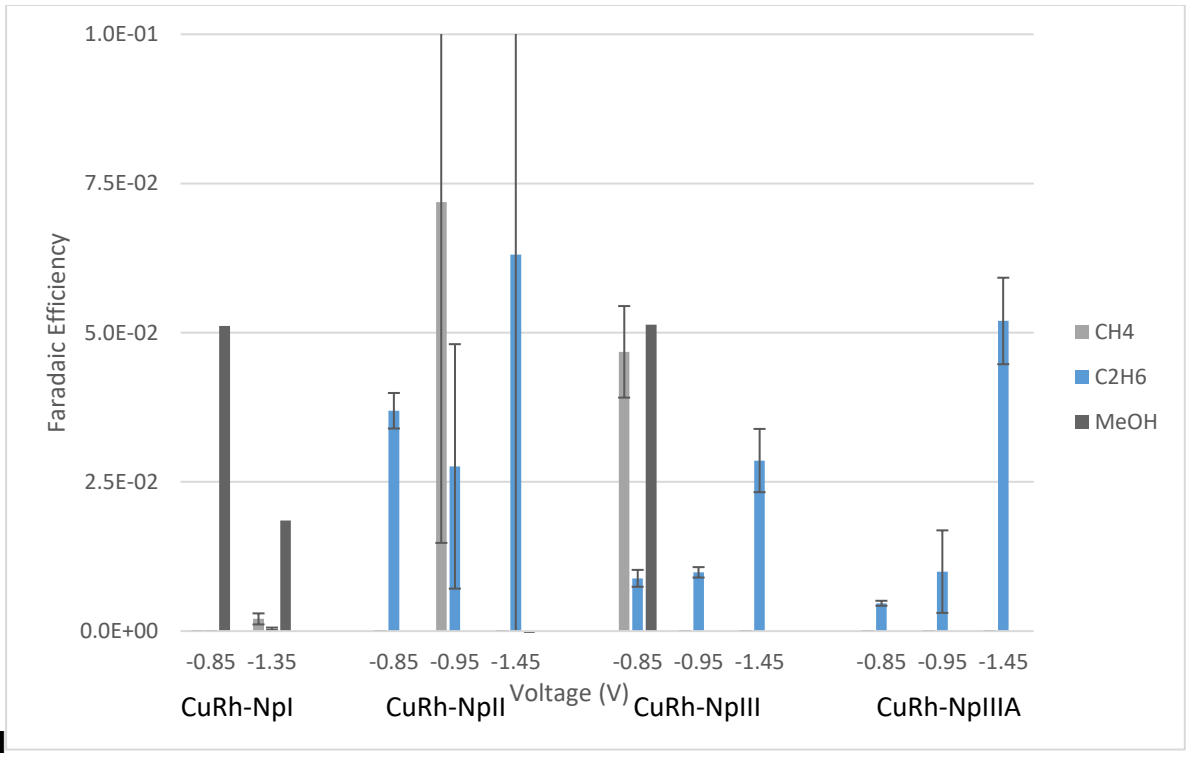

H

Figure 11: graphs A-D show product formation rates in mol/(min x cm^2), while E-H show product selectivity measured in Faradaic Efficiency. Catalyst surface area was 26 cm^2, experiments were done at room temperature, DSA was used as a counter electrode, and RHE was used as a reference. No gas data was obtained for the CuRh-NpI experiment at -0.85 V due to an error in GC setup. The gas data of four experiments (CuRh-NpI at -1.35 V, and CuRh-NpII at -0.85, -0.95, and -1.45 V) was normalized so that total FE came to 100% due to CO_2 flow rate measurement issues; liquid quantification was unaffected for these experiments.

The rhodium copper catalyst CuRh-NpII was about 25% covered by particles. These included small growths of well defined particulate structures and larger, rounded, translucent blobs. The particulate structures were about 0.5-2 microns in diameter, and included small blocky particles with side lengths of about 75 nm. Rounded particles in these growths were slightly smaller, with diameters of around 50 nm. The background exhibits interesting contrast, with some swaths lighter than others. Clear images showing background particle sizes were not obtained. Three spots were used for EDX, with two on the particulate structures and one on the background. Rhodium was detected in all three spots, at weight percentages of 0.35%, 0.31%, and 0.21%. Interestingly, this sample also revealed carbon, oxygen, and fluorine, but not aluminum. Again, a higher amount of rhodium correlated with a higher amount of other elements.

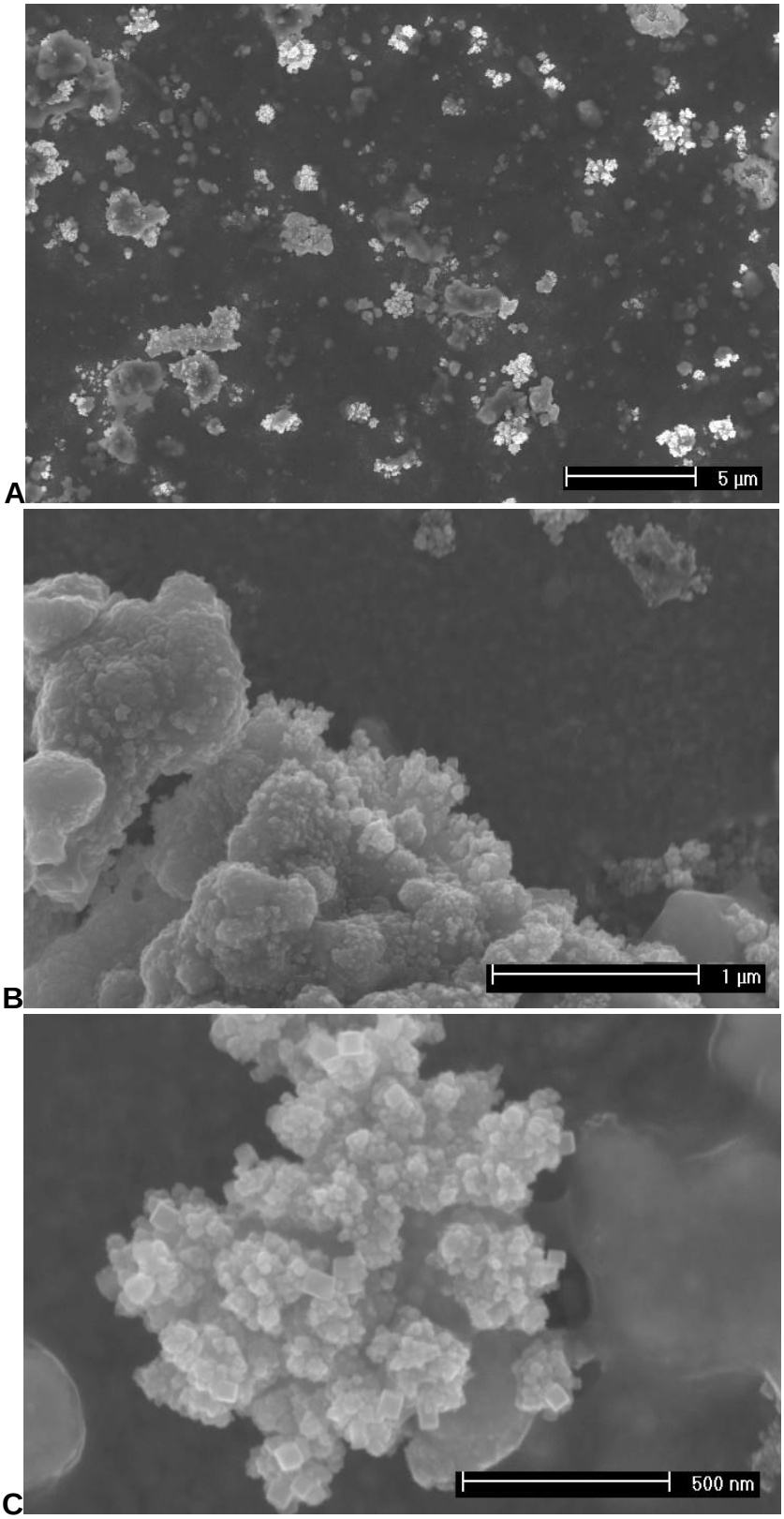

Figure 12: SEM images of catalyst CuRh-NpII. Image A is 1600x magnification, image B is 25600x magnification, and image C is 51200x magnification.

Like those for CuRh-NpII, SEM images of catalyst CuRh-NpIII exhibit similar large, translucent blob structures, but its more defined particulate structures lack the blocky particles of the last catalyst. The background included light and dark swaths, just like the other rhodium catalyst. Particles on the surface appeared slightly smaller than those of the CuIr catalyst, ranging from about 40-70 nm. The space between the particles was also larger, ranging up to 30 nm in some places. The EDX spots show small amounts of rhodium present on the two spots on particulate structures chosen and on the background spot (0.85, 0.40, and 0.06 wt%). The same contaminants were present for this sample as the last rhodium catalyst, however more were observed at the spot with 0.40 wt% than at the 0.80% rhodium spot.

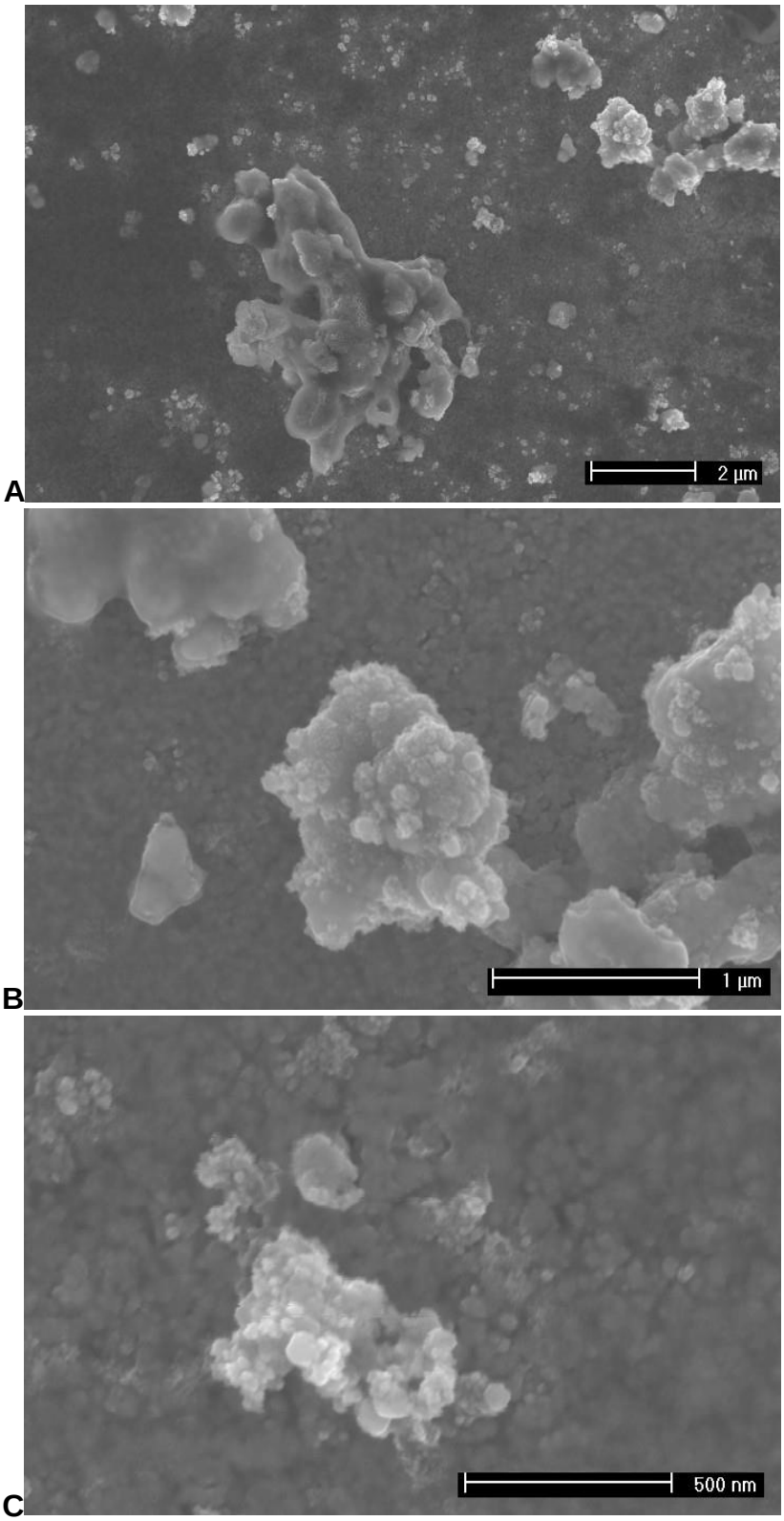

Figure 13: SEM images of catalyst CuRh-NpIII. Image A is at 6400x magnification, image B is at 25600x magnification, and image C is at 51200x magnification.

Data from the CuRh catalysts suffer from reproducibility issues. These were the first catalysts made as part of this project, and it is possible that these catalysts differ as the result of inconsistent laboratory technique in the process of adding copper nanoparticles to the catalyst. However, catalysts CuRh-NpIII and CuRh-NpIIIA were prepared concurrently, and still show differing reaction trends. There are several other reasons why the reaction trends of these catalysts may differ. For the NpIII and NpIIIA catalysts specifically, age of the catalyst may have been a factor; the experiments for NpIII were completed around a month after creation, whereas those for NpIIIA were completed when the catalyst was almost two months old. Just like nanoporous copper catalysts seem to undergo activation through use, the rhodium copper surface may slowly adjust to a more stable structure over time. The differences in reaction trends may also relate to the GC system. For most of these experiments, the CO_2 flow rate decreased as the experiment went on. Decreased CO_2 flow affects the solvation rate of CO_2, which can in turn affect reaction rates for different products.

Two features stand out in the SEM images for rhodium copper catalysts: the smooth, translucent structures and the angular particles on opaque clump surfaces. Catalyst CuRh-NpII, which displayed the angular particles, differed from the other catalysts of several of the liquid products. It produced much higher levels of formate at the two lower voltages tested, produced acetate at both -0.95 and -1.45 V, produced ethanol at -1.45 V, and was the only of the rhodium copper catalysts to produce detectable levels of propanol. Further experiments could strengthen the association between the angular particles and the formation of these liquid products.

The translucent structures shown in the rhodium copper SEM images may be the result of Nafion, the binding agent used in anchoring copper nanoparticles to the surface. It's possible that the Nafion may affect the reactions by blocking active sites, or alter the creation of bimetallic catalysts by blocking the galvanic displacement of copper particles by other metals.

4.2 Iridium Copper Catalysts

Two different iridium copper catalysts were produced, the first with more iridium than the latter. The first of the iridium copper catalysts, CuIr-NpI, produced a high amount of formate fairly consistently across the spectrum of potentials used for experiment. The amount of hydrogen produced increased with greater negative potential. Carbon monoxide production peaked at -1.25 V, but in terms of Faradaic Efficiency it tended to decrease with more negative potential. Both ethylene and ethane followed the same pattern, also peaking at -1.25 V, though their Faradaic Efficiencies arced, rather than linearly decreased with negative potential. No methane, methanol, or propanol was observed to be produced, and ethanol was only observed in one instance.

The second iridium copper catalyst, CuIr-NpII, was very different from the other iridium copper catalyst. The most obvious difference was that CuIr-NpII produced currents 1.5-2.5 mA/cm^2 higher than CuIr-NpI. The next obvious difference was in hydrogen and formate production. CuIr-NpII produced a much lower amount of formate and higher amount of hydrogen than the previous catalyst, especially comparing Faradaic Efficiencies. Carbon monoxide was produced at about the same level as in the previous catalyst, although instead of peaking at -1.25 V, production dropped at this potential and was at a maximum at -1.45 V. Ethane and ethylene were produced at similar levels to the last catalyst, though there was no correlation with potential. This catalyst produced ethanol in all trials done at potentials more negative than -1.05 V, although no trend was observed. This catalyst did not produce methane, methanol, propanol, or acetate.

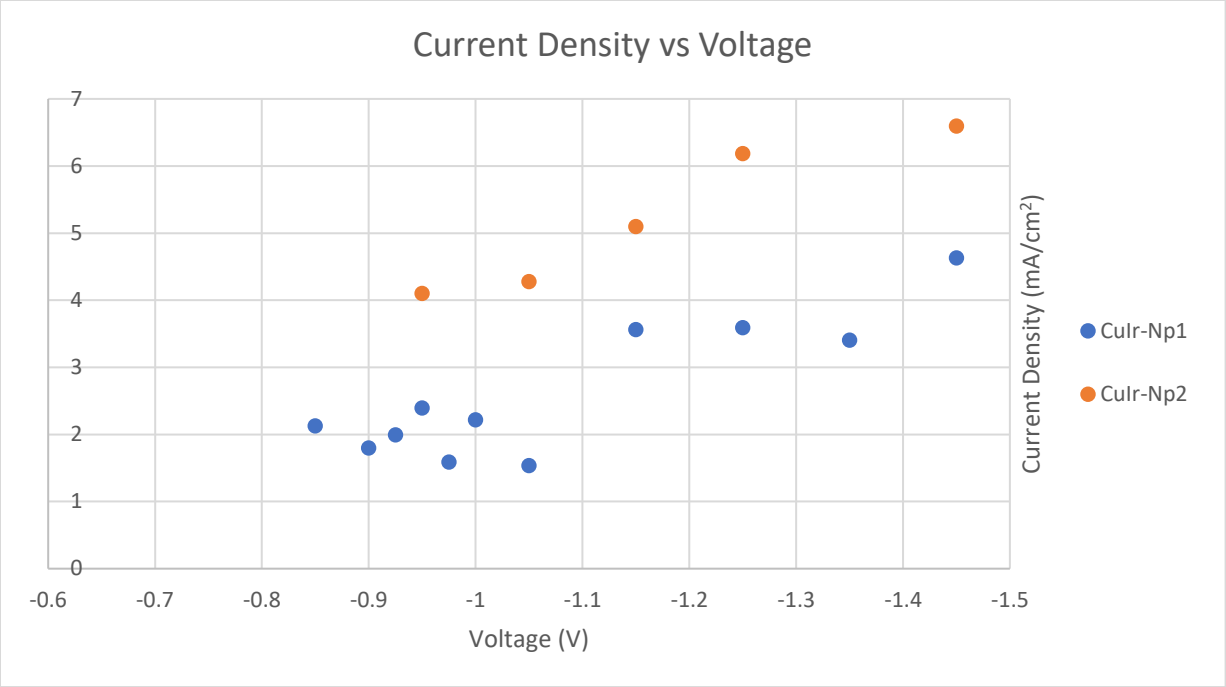

Figure 14: Average current densities of iridium copper catalysts plotted versus voltage. Current densities for the second catalyst are consistently higher.

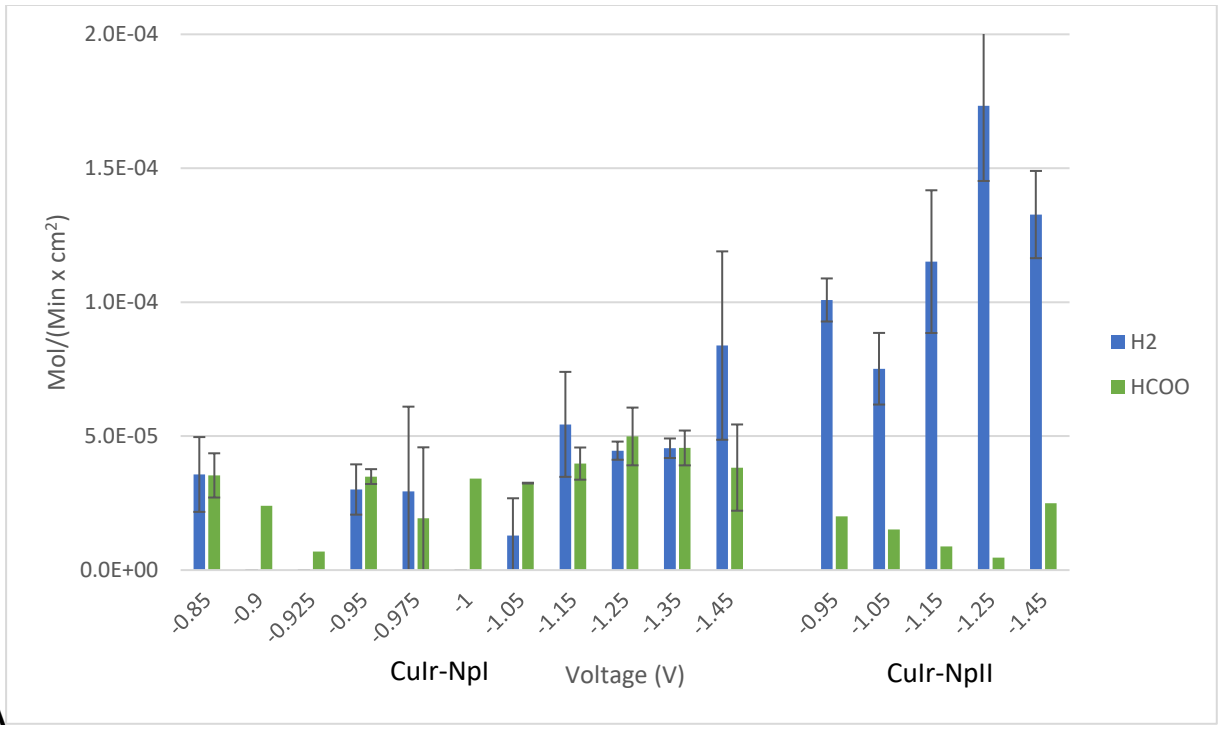
2.0E-04
1.5E-04
1.0E-04
5.0E-05
0.0E+00
Mol/(Min x cm²)
H2
HCOO
-0.85
-0.9
-0.925
-0.95
-0.975
-1
-1.05
-1.15
-1.25
-1.35
-1.45
-0.95
-1.05
-1.15
-1.25
-1.45
CuIr-NpI
Voltage (V)
CuIr-NpII

A

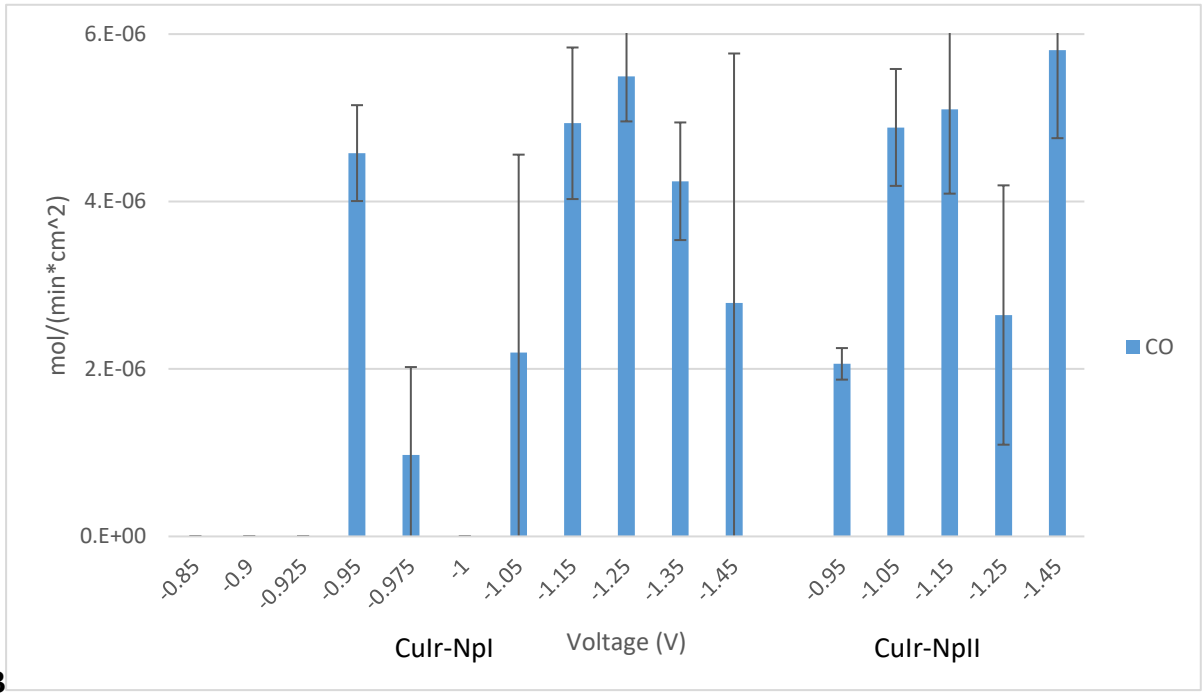
6.E-06
4.E-06
2.E-06
0.E+00
mol/(min*cm^2)
CO
-0.85
-0.9
-0.925
-0.95
-0.975
-1
-1.05
-1.15
-1.25
-1.35
-1.45
-0.95
-1.05
-1.15
-1.25
-1.45
CuIr-NpI
Voltage (V)
CuIr-NpII

B

C

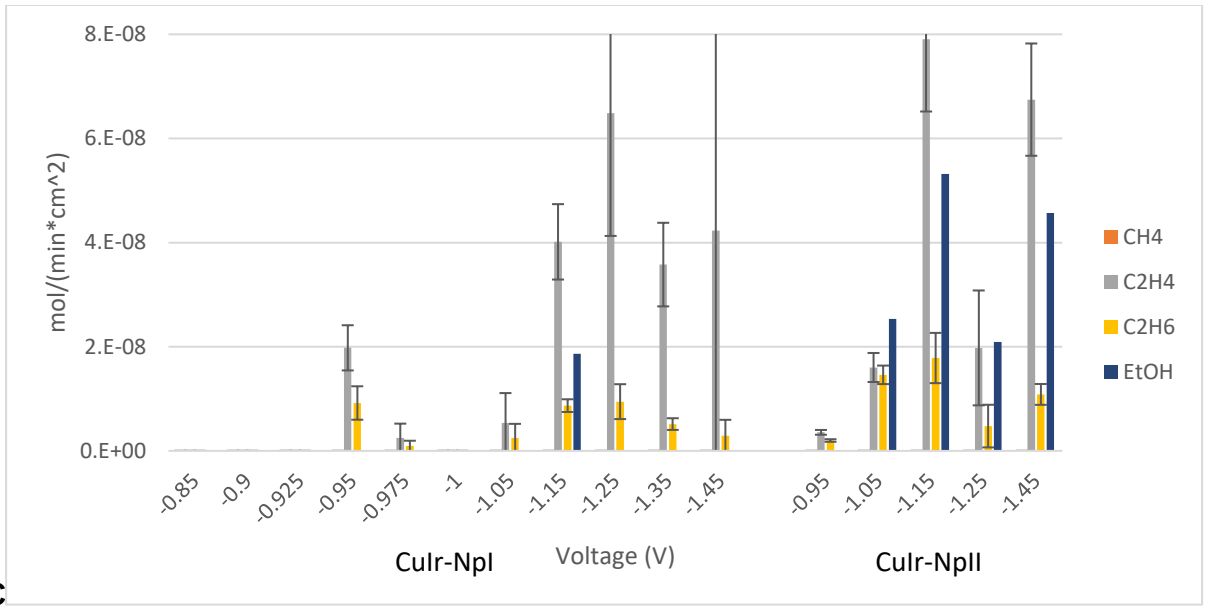
8.E-08
6.E-08
4.E-08
2.E-08
0.E+00
mol/(min*cm^2)
CH4
C2H4
C2H6
EtOH
-0.85
-0.9
-0.925
-0.95
-0.975
-1
-1.05
-1.15
-1.25
-1.35
-1.45
-0.95
-1.05
-1.15
-1.25
-1.45
CuIr-NpI
Voltage (V)
CuIr-NpII

D

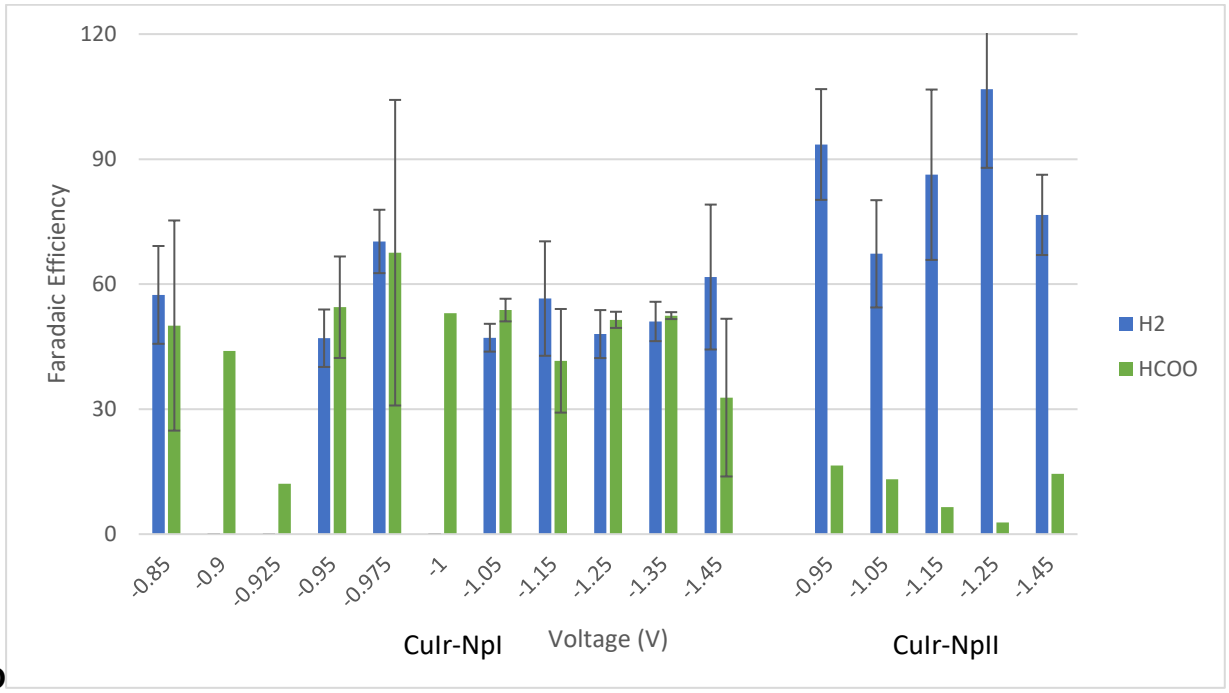
120
90
60
30
0
Faradaic Efficiency
H2
HCOO
-0.85
-0.9
-0.925
-0.95
-0.975
-1
-1.05
-1.15
-1.25
-1.35
-1.45
-0.95
-1.05
-1.15
-1.25
-1.45
CuIr-NpI
Voltage (V)
CuIr-NpII

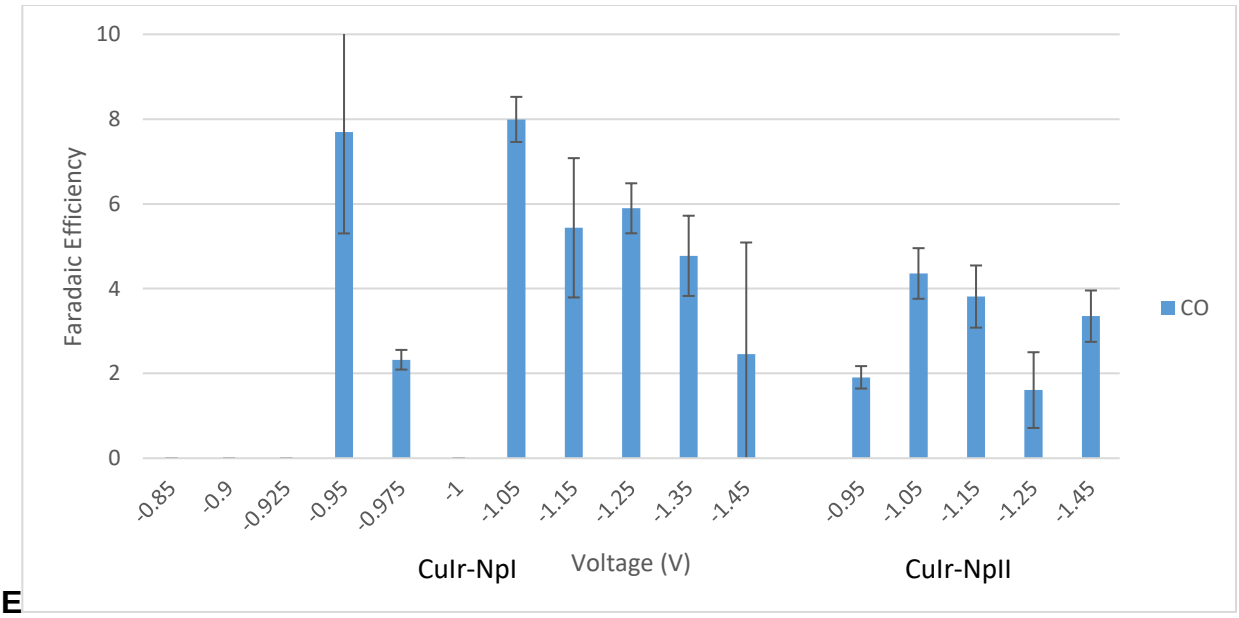

E

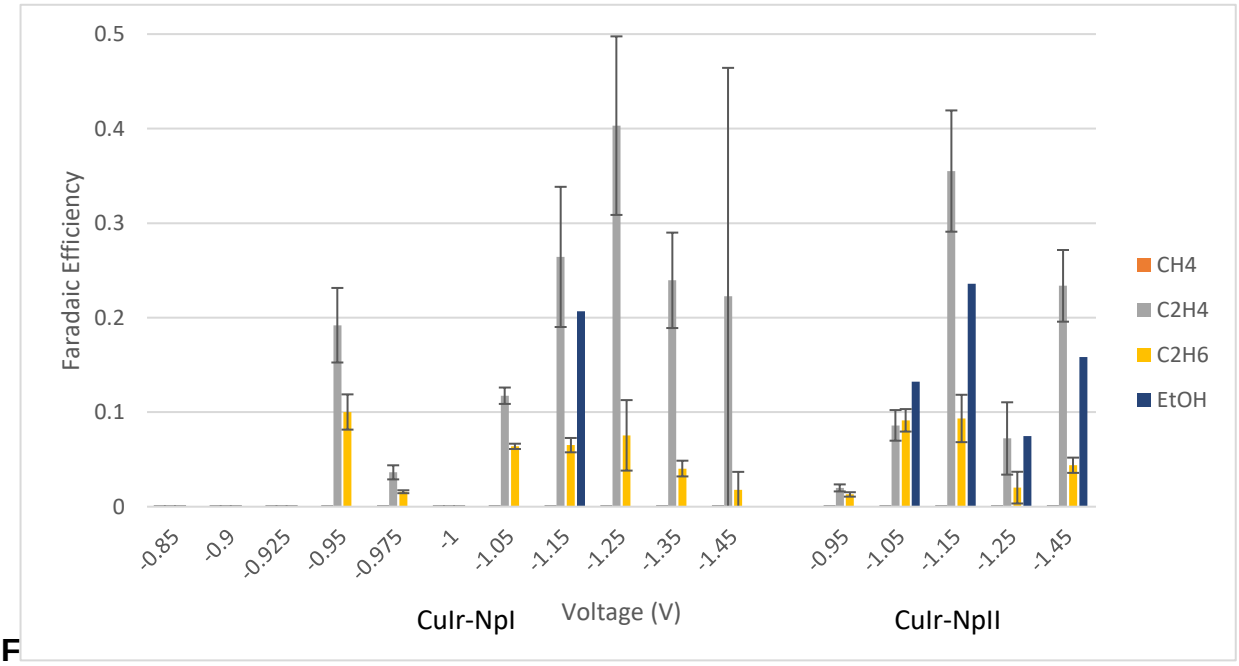

F

Figure 15: Graphs A-C show product formation rates in mol/(min x cm^2), while D-F show product selectivity in Faradaic Efficiency. Experiments were done at room temperature using 0.1 M $KHCO_3$ electrolyte saturated with CO_2 gas. Catalyst surface area was 26 cm^2, DSA was used as a counter electrode, and RHE was used as a reference. For three experiments – CuIr-NpI at -0.9, -0.925, and -1 V – the GC was down and gaseous data was not collected.

SEM and EDX data was obtained for one of the iridium copper catalysts (CuIr-Np) and two of the rhodium copper catalysts (CuRh-NpII and CuRh-NpIII). The images of the iridium copper catalyst showed about 50% coverage of the catalyst surface with particles. The largest clumps, which were rare, measured up to 15 microns in diameter and were not round. Close examination of these clumps showed a textured surface covered with particles about 75 nm in diameter. These small particles were rather flat in some cases, but as can be seen in figure 16, some structures seemed to be made up of smoother, more spherical particles, also about 75 nm in diameter. The dark background looks like a relatively flat surface made up of round particles around 50-80 nm in diameter. EDX data was obtained from three spots on the iridium catalyst; two of these were on clumps of particles, and one was on the dark background. Both of the EDX spots from particles showed iridium peaks, which were calculated to be 3.41 and 2.38 wt% of the elemental makeup. Iridium peaks were also present in the spectrum from the background spot, though they were not quantified. All three spots showed peaks due to carbon, oxygen, fluorine, and aluminum (in addition to copper). Contamination was much less on the background spot than on the foreground spots for each element. Spots focused further from the catalyst surface had a higher amount of contamination, as well as iridium.

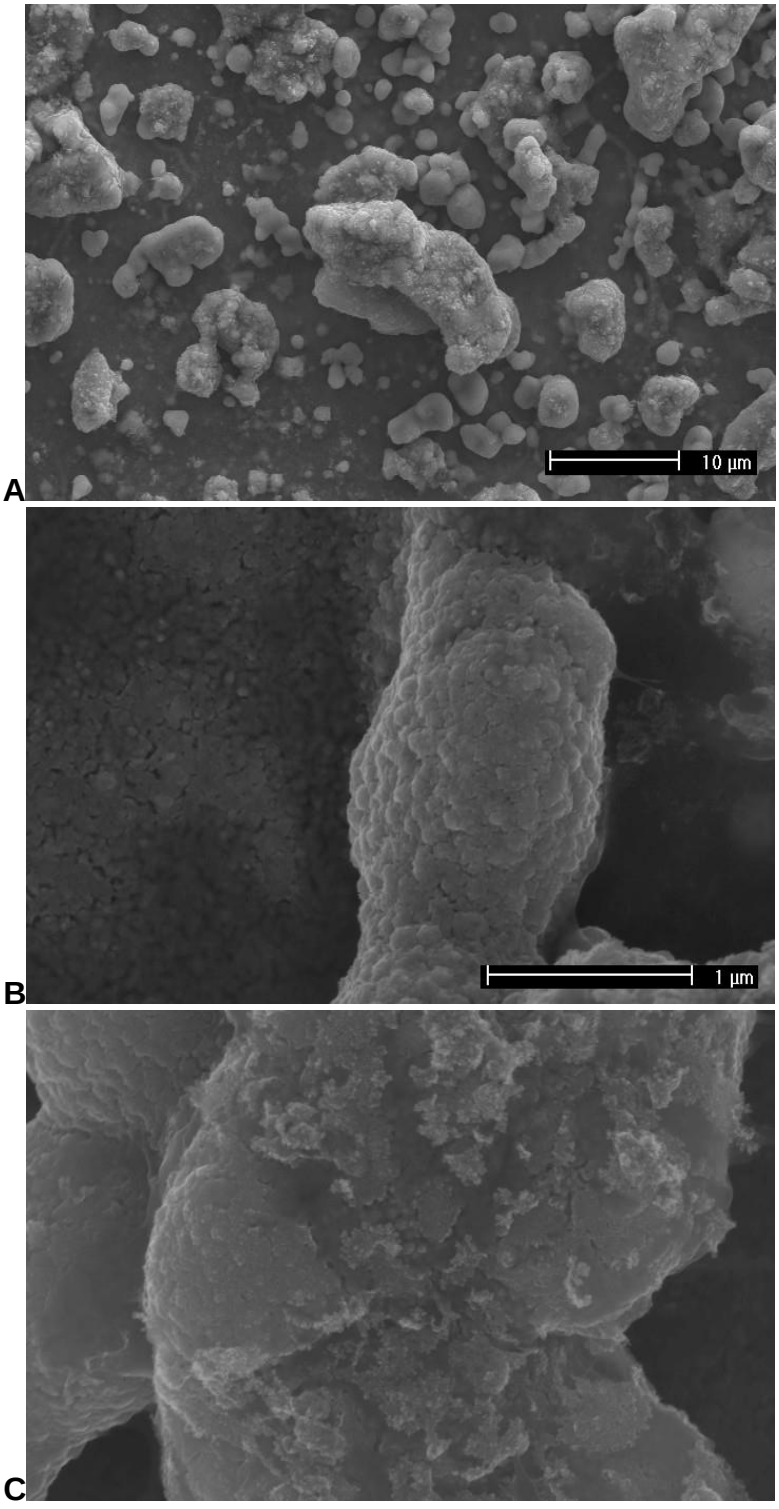

Figure 16: SEM images of CuIr-NpI. Image A is at 1600x magnification, image B is 25600x magnification, and image C is 25600x magnification.

Because CuIr-NpI was immersed in a more concentrated $IrCl_3$ solution than CuIr-NpII, it is assumed that CuIr-NpI has more iridium on its surface than CuIr-NpII. Based on this, several points are evident. First, greater incorporation of iridium has an inhibitory effect on hydrogen production. CuIr-NpII's rate of hydrogen production was at least twice as much as NpI's at every potential. Second, a higher concentration of iridium led to lower current density. As shown in figure 14, NpII consistently generated current densities much higher than NpI's. This is likely the direct result of increased hydrogen activity. For most other products, the difference of iridium concentration seems not to have made a difference, with formate and ethanol being the exceptions. Levels of formate produced by NpI were much higher than those of NpII. However, NpII was able to produce ethanol when NpI could not. Again, this information suggests the possibility that NpII had active sites that converted formate to ethanol. This is another question that could be investigated with ^{13}C experiments. Otherwise, reaction trends for the two catalysts were similar.

4.3 Comparison of Bimetallic Catalysts to Nanoporous Copper Catalysts

Generally, the bimetallic catalysts produced higher current densities than simple nanoporous copper catalysts but were less likely to produce larger molecules. This is especially apparent with CuIr-NpI, which produced formate with high selectivity, but produced no alcohols (with the exception of ethanol in a single trial) or acetate and very little ethane or ethylene. CuIr-NpII, which had less iridium, produced substantially larger current densities as the result of increased hydrogen activity. Specific conclusions are hard to draw from the rhodium copper data, although it also demonstrated higher selectivity for formate and lower selectivity for other products.

5 Conclusions

Product formation rates between several catalysts were done at -1.45 V. Figure 17 shows the generation of C2 and C3 products produced by the most successful catalysts. As can be seen, the mortar and pestle catalyst generated much more ethylene, acetate, ethanol, and propanol than other catalysts.

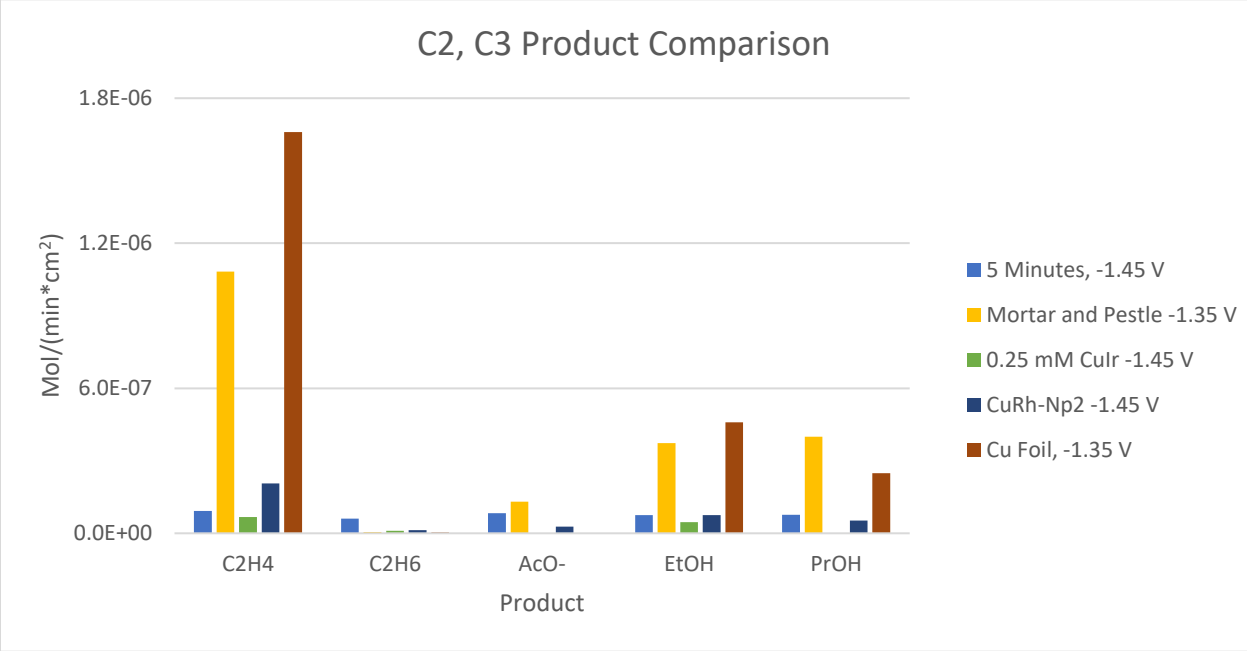

Figure 17: production rates of higher order hydrocarbons by five catalysts at -1.45 V, with the exception of the mortar and pestle catalyst and Cu foil, which were tested at -1.35 V. All experiments were an hour long, run at room temperature, using 0.1 M $KHCO_3$ as electrolyte. Catalyst surface area was 26 cm^2, DSA was used as a counter electrode, and RHE was used as a reference. For the Cu foil data, fresh electrolyte was also flowed through the working compartment of the cell.

The ball-milled nanoporous copper experiments demonstrated how particle size affects product distribution trends for nanoporous copper catalysts. Among the ball-milled catalysts, 97A produced the highest amounts of non hydrogen products, and was the only ball-milled catalyst to produce propanol. Catalysts 97B and 97C, which experienced more milling, produced decreasing amounts of non hydrogen products, showing that increased milling decreased analyte production. At the same time, catalyst 97B produced the highest current density of the three catalysts, and catalyst 97C produced a current density within 10% of 97A's. This is puzzling because SEM images of the three catalysts show that the surface of 97A was densely coated with 3D particle structures, while the other two catalysts were not nearly as well covered.

This suggests that the structures present on 97A were not as active in hydrogen formation as elements that were present in the other two catalysts. It is possible that the surface floor of the catalyst was most active in hydrogen formation. Decreased particle coverage on catalysts 97B and 97C allowed greater solution access to the floor of the catalyst. In addition, 97B's surface was noted to be rougher than that of 97C, which would increase the surface area of the floor, allowing greater hydrogen production. As for the difference in production between 97A and 97C, it was hard to see the floor of 97A, but it is expected that the same particles present on the structure surfaces would also have been deposited on the catalyst floor, giving parts of it similar roughness to 97B. This influence, tempered by poor access of solution to the floor, could explain why 97A still produced more hydrogen than 97C.

The nanoporous catalyst NpCu MP was made by depositing copper particles ground in a mortar and pestle onto clean copper foil. The most obvious trend for this catalyst was that higher order carbon products were more common at higher voltages. This suggests that C_1 products may be involved in the formation of C_2 products, as their productions seemed to have an inverse relationship. This trend did not continue with C_3 products in the potentials tested, although C_3 products were only measured at -1.05 V and lower, and did increase with negative voltage.

Rhodium copper catalysts suffered from lack of reproducibility. Since these were the first catalysts made as part of this independent project, it's possible that the production process was inconsistent, leading to unexpected differences between the catalysts. Instability of flow rate also contributed to inconsistent data. Every rhodium copper catalyst produced hydrogen, formate, carbon monoxide, ethylene, and ethane. Methane, methanol, ethanol, propanol, and acetate were also produced, but not by every catalyst, and not by a discernable trend.

The iridium copper catalysts produced hydrogen, formate, carbon monoxide, ethylene, ethane, and ethanol. For the copper made in more concentrated $IrCl_3$ solution, formate was produced in very high FE's across the voltage range. Ethanol was detected at only one voltage (-1.15 V). The catalyst immersed in diluted $IrCl_3$ displayed a higher current density and much higher

production of hydrogen. This catalyst also produced much less formate, but did produce ethanol at every potential more negative than -1.05. This catalyst's production of ethane and ethylene seemed to peak at lower potential's than the first iridium copper catalyst.

As shown in figure 18, NpCu MP had the lowest current density of all the catalysts at almost every voltage. While current density is a good measure of the amount of reactions taking place, NpCu MP's low current density does not make it a bad catalyst. On the contrary, this catalyst had the lowest hydrogen production of any of the catalysts and also produced the most C_2 and C_3 products at large voltages. At -1.35 V, NpCu MP produced almost 10x the C_2 products of any of the other catalysts. It was also the only catalyst to produce propanol at a potential greater than -1.15 V. That said, the catalyst CuIr-NpI was a standout for its formate selectivity and activity. The catalyst's FE for formate reached 54% at -0.95 V, higher than any other tested catalyst's FE for any product other than hydrogen.

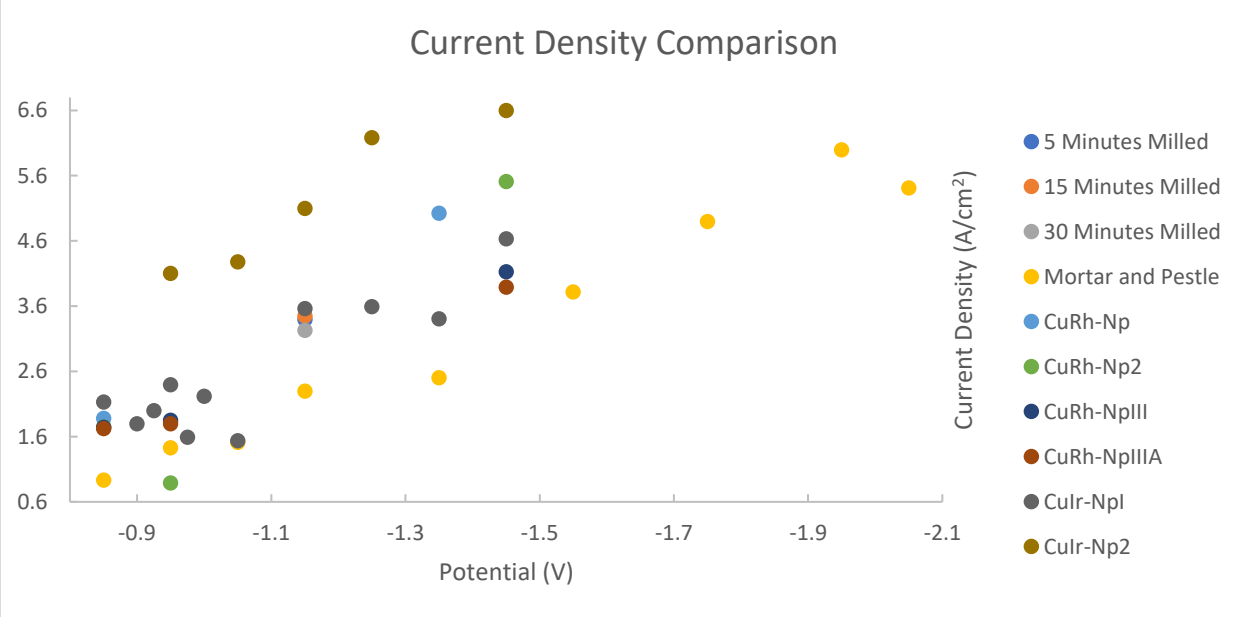

Figure 18: a comparison of current densities for all tested catalysts at all voltages tested. All experiments were an hour long, run at room temperature, using 0.1 M $KHCO_3$ as electrolyte. Catalyst surface area was 26 cm^2, DSA was used as a counter electrode, and RHE was used as a reference.

Altering the nanoporous copper catalysts did not allow the catalysts to produce any products not seen at similar voltages for NpCu MP. At the levels they were incorporated, iridium and rhodium were more effective at decreasing hydrocarbon production, with the exception of formate.

6 References

1. Karl, T; Schmidt, G. NOAA/NASA 2013 Global Temperatures (Jan 21, 2014). http://www.nasa.gov/sites/default/files/files/NOAA_NASA_2013_Global_Temperatures_Joint_Briefing.pdf (accessed Feb 2, 2015).
2. Dr. Pieter Tans, NOAA/ESRL (www.esrl.noaa.gov/gmd/ccgg/trends/) and Dr. Ralph Keeling, Scripps Institution of Oceanography (scrippsco2.ucsd.edu/). Accessed Feb 9, 2015.
3. Boden, T.A., G. Marland, and R.J. Andres. 2010. Global, Regional, and National Fossil-Fuel CO_2 Emissions. Carbon Dioxide Information Analysis Center, Oak Ridge National Laboratory, U.S. Department of Energy, Oak Ridge, Tenn., U.S.A. doi 10.3334/CDIAC/00001_V2010.
4. Hori, Y.; Kikuchi, K.; Suzuki, S. Production of CO and CH_4 in Electrochemical Reduction of CO_2 at Metal Electrodes in Aqueous Hydrogencarbonate Solution. Chem. Lett. 1985, 1695-1698.
5. Kuhl, K.; Cave, E.; Abram, D.; Jaramillo, T. New Insights into the Electrochemical Reduction of Carbon Dioxide on Metallic Copper Surfaces. Energy Environ. Sci., 2012, 5, 7050.

7 Acknowledgments

I would like to thank Dr. Anne Co for her unwavering mentorship and generosity over the past three years. I consider myself very lucky to be a part of this great group.

I also wish to extend thanks to Joshua Billy, my graduate student mentor, who developed the procedure I have centered this project on. His insight and expertise with our instruments was incredibly helpful, and he was the driving force behind the SEM and EDX data collection.